

ELEMENTAL ABUNDANCE RATIOS IN STARS OF THE OUTER GALACTIC DISK. IV. A NEW SAMPLE OF OPEN CLUSTERS¹

DAVID YONG

Research School of Astronomy and Astrophysics, Australian National University, Weston, ACT 2611, Australia; yong@mso.anu.edu.au

BRUCE W. CARNEY

Department of Physics & Astronomy, University of North Carolina, Chapel Hill, NC 27599-3255, USA; email: bruce@physics.unc.edu

EILEEN D. FRIEL

Department of Astronomy, Indiana University, Bloomington, IN 47405, USA; email: efriel@indiana.edu

Draft version July 2, 2012

ABSTRACT

We present radial velocities and chemical abundances for nine stars in the old, distant open clusters Be 18, Be 21, Be 22, Be 32, and PWM 4. For Be 18 and PWM 4, these are the first chemical abundance measurements. Combining our data with literature results produces a compilation of some 68 chemical abundance measurements in 49 unique clusters. For this combined sample, we study the chemical abundances of open clusters as a function of distance, age, and metallicity. We confirm that the metallicity gradient in the outer disk is flatter than the gradient in the vicinity of the solar neighborhood. We also confirm that the open clusters in the outer disk are metal-poor with enhancements in the ratios $[\alpha/\text{Fe}]$ and perhaps $[\text{Eu}/\text{Fe}]$. All elements show negligible or small trends between $[\text{X}/\text{Fe}]$ and distance (< 0.02 dex/kpc), but for some elements, there is a hint that the local ($R_{\text{GC}} < 13$ kpc) and distant ($R_{\text{GC}} > 13$ kpc) samples may have different trends with distance. There is no evidence for significant abundance trends versus age (< 0.04 dex Gyr⁻¹). We measure the linear relation between $[\text{X}/\text{Fe}]$ and metallicity, $[\text{Fe}/\text{H}]$, and find that the scatter about the mean trend is comparable to the measurement uncertainties. Comparison with solar neighborhood field giants shows that the open clusters share similar abundance ratios $[\text{X}/\text{Fe}]$ at a given metallicity. While the flattening of the metallicity gradient and enhanced $[\alpha/\text{Fe}]$ ratios in the outer disk suggest a different chemical enrichment history to the solar neighborhood, we echo the sentiments expressed by Friel et al. that definitive conclusions await homogeneous analyses of larger samples of stars in larger numbers of clusters. Arguably, our understanding of the evolution of the outer disk from open clusters is currently limited by systematic abundance differences between various studies.

Subject headings: Galaxy: abundances, Galaxy: disk, Galaxy: open clusters and associations: general

1. INTRODUCTION

Our Galaxy's open clusters are valuable tools to study the disk (Friel 1995). Accurate homogeneous distances and ages can be measured for samples of open clusters that span a wide range in parameters (Salaris et al. 2004). Additionally, metallicity estimates of open clusters can be readily obtained from a variety of methods (albeit with differing degrees of accuracy) thereby enabling studies of the structure, kinematics, and chemistry of the disk as well as any temporal variations of these properties.

The atmospheres of low-mass stars retain, to a great extent, the chemical composition of the interstellar medium at the time and place of their birth. The nucleosynthetic yields of the chemical elements depend upon stellar mass and metallicity. Therefore, measurements of metallicity, $[\text{Fe}/\text{H}]$, and chemical abundance ratios, $[\text{X}/\text{Fe}]$, in stars in open clusters offer powerful insight into the formation and evolution of the disk (Janes 1979; Freeman & Bland-Hawthorn 2002; Friel et al. 2002; Bland-Hawthorn et al. 2010; Kobayashi & Nakasato 2011).

In recent times there has been considerable effort to under-

stand the evolution of the outer Galactic disk (e.g., Hou et al. 2000; Chiappini et al. 2001; Andrievsky et al. 2002c; Daflon & Cunha 2004; Costa et al. 2004; Cescutti et al. 2007; Magrini et al. 2009). It appears that the metallicity gradient (i.e., $[\text{Fe}/\text{H}]$ versus Galactocentric distance, R_{GC}) in the outer disk ($R_{\text{GC}} > 13$ kpc) is flatter than the metallicity gradient in the solar neighborhood (e.g., Twarog et al. 1997; Luck et al. 2003; Carraro et al. 2004; Carney et al. 2005b; Yong et al. 2005; Bragaglia et al. 2008; Sestito et al. 2008; Jacobson et al. 2009; Friel et al. 2010). Qualitatively similar behavior has now been found in external galaxies (e.g., Worthey et al. 2005; Bresolin et al. 2009; Vlajić et al. 2009, 2011) suggesting that the processes which govern chemical evolution in the outer Galactic disk have also operated in the outskirts of other disk galaxies.

Another intriguing result is evidence for enhanced $[\alpha/\text{Fe}]$ ratios in the outer Galactic disk from open clusters (Carraro et al. 2004; Yong et al. 2005), field stars (Carney et al. 2005b; Bensby et al. 2011), and Cepheids (Yong et al. 2006). Such abundance ratios in objects spanning a large range in ages can be explained by infall of pristine gas in the outer disk and/or vigorous star formation. Either explanation requires that the outer disk has experienced a significantly different star formation history compared to the solar neighborhood and this has important implications for the formation and evolution of the Galactic disk.

¹ The data presented herein were obtained at the W.M. Keck Observatory, which is operated as a scientific partnership among the California Institute of Technology, the University of California and the National Aeronautics and Space Administration. The Observatory was made possible by the generous financial support of the W. M. Keck Foundation.

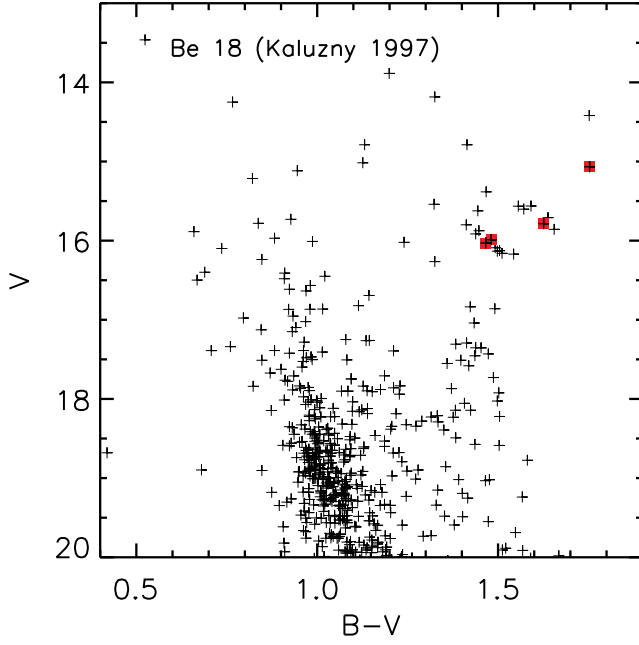


FIG. 1.— Be 18 color-magnitude diagram using the data from Kaluzny (1997). We distinguish our program stars by red squares.

However, not all studies of the outer disk find enhanced $[\alpha/\text{Fe}]$ ratios (e.g., Bragaglia et al. 2008). While one explanation for the discrepancy may be systematic differences in the analyses, studies of additional open clusters in the outer disk are necessary to clarify the situation. Therefore, to further explore the formation and evolution of the outer Galactic disk, we analyze the chemical abundances of a new sample of open clusters. This is the fourth, and final, paper in our series on elemental abundance ratios in stars in the outer Galactic disk. Paper I (Yong et al. 2005) concentrated upon open clusters, Paper II (Carney et al. 2005b) was dedicated to field red giants, and Paper III (Yong et al. 2006) focused upon Cepheids. In this paper, we present radial velocities, metallicities $[\text{Fe}/\text{H}]$, and element abundance ratios $[\text{X}/\text{Fe}]$ for the open clusters Be 18, Be 21, Be 22, Be 32, and PWM 4.

2. PROGRAM STARS AND OBSERVATIONS

2.1. Target Selection

We searched the WEBDA database² and the recent literature to identify additional old (> 2 Gyr), distant ($R_{\text{GC}} > 10$ kpc) open clusters. The following open clusters were identified as suitable candidates: Be 18, Be 21, Be 22, Be 32, and PWM 4. Following our approach in Paper I, individual stars were selected from optical and infra-red color-magnitude diagrams (see Figures 1 to 10 and Tables 1 and 2). For Be 32, D’Orazi et al. (2006) measured radial velocities for a large sample of stars and thus we were able to select likely members for this cluster.

2.2. Observations and Data Reduction

We used the HIRES (Vogt et al. 1994) spectrograph on the Keck I Telescope on 12 November 2006 and 27 December 2006. On both occasions we used the red cross-disperser and the B5 decker which has a slit width of $0''.86$ and a slit length

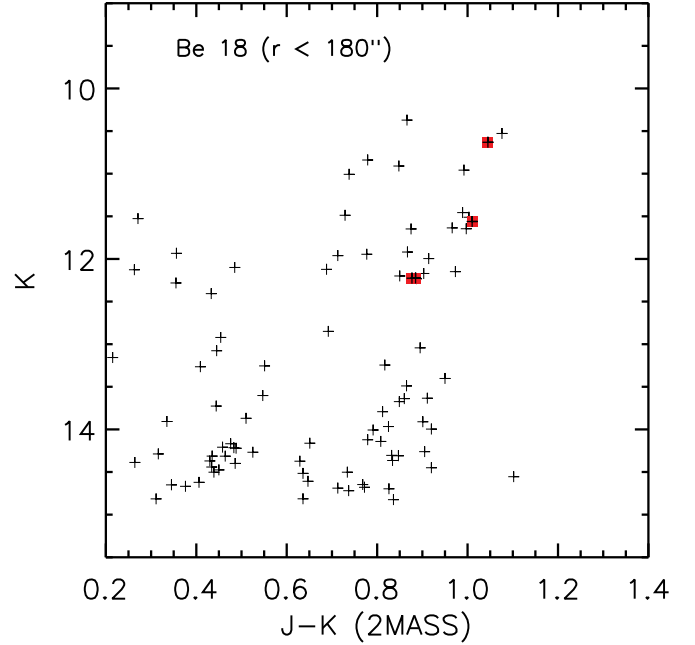


FIG. 2.— Be 18 color-magnitude diagram using the data from 2MASS Skrutskie et al. (2006). We distinguish our program stars by red squares.

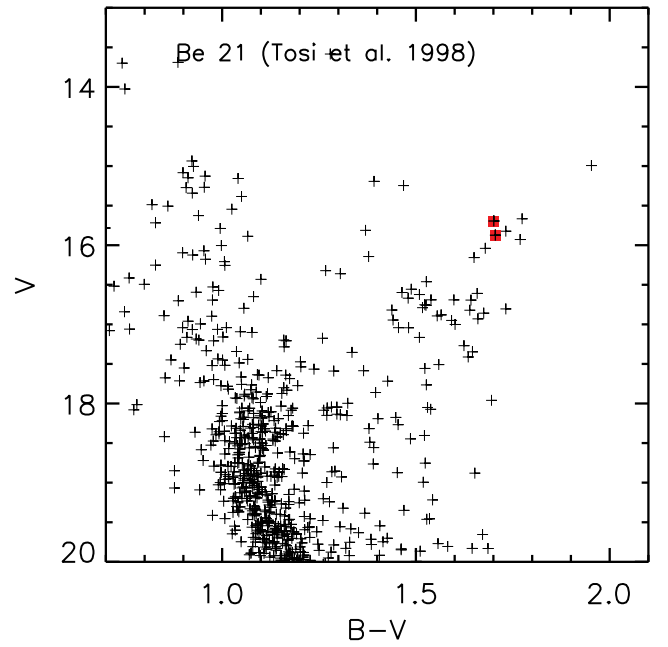


FIG. 3.— Be 21 color-magnitude diagram using the data from Tosi et al. (1998). We distinguish our program stars by red squares.

of $3''.5$. On the November run, we binned the CCD 3×1 (spatial \times spectral) and on the December run we binned the CCD 2×1 . The observing routine included 20 quartz lamp exposures for flat fielding as well as 20 zero second exposures for “bias” frames. ThAr frames were taken during each night (three on 12 November and eight on 27 December) and two radial velocity standards were observed on each night. The

² <http://www.univie.ac.at/webda/>

TABLE 1
OBSERVED CLUSTERS

Cluster	R.A. ^a (J2000)	Decl. ^a (J2000)	ℓ^a	b^a	[Fe/H] ^a	δV^b	MAI ^c	d ^d	d ^e
Berkeley 18	05:22:12	+45:24:00	163.63	+5.02	+0.02	2.3	5.69	5.8	5.4
Berkeley 21	05:51:42	+21:47:00	186.84	-2.51	-0.83	1.6	2.18	5.0	6.2
Berkeley 22	05:58:24	+07:50:00	199.88	-8.08	-0.30	2.1	4.26	7.7	6.2
Berkeley 32	06:58:06	+06:26:00	207.95	+4.40	-0.58	2.4	5.91	3.1	3.2
PWM 4	23:50:55	+62:19:15	115.96	+0.27	...	3.0	7.00 ^f	7.9 ^f	7.2

^a Taken from WEBDA.

^b Taken from Salaris et al. (2004).

^c Taken from Salaris et al. (2004), in Gyrs.

^d Distance in kpc from Salaris et al. (2004).

^e Distance estimate obtained using red clump stars (this paper).

^f Taken from Ortolani et al. (2005)

TABLE 2
PHOTOMETRIC DATA

Star	R.A. ^a (J2000)	Decl. ^a (J2000)	V	$B-V$	$V-I_C$	K^a	$J-K^a$	Reference
Be18 532	05 22 13.7	+45 25 46.8	15.99	1.48	1.68	12.226	0.877	1
Be18 1006	05 22 16.2	+45 27 28.5	16.03	1.47	1.70	12.224	0.885	1
Be18 1163	05 22 13.8	+45 27 58.9	15.79	1.63	1.86	11.561	1.010	1
Be18 1383	05 22 10.7	+45 28 49.4	15.07	1.75	1.94	10.631	1.045	1
Be21 T50	05 51 42.3	+21 48 45.4	15.87	1.71	2.07	11.142	1.062	2
Be21 T51	05 51 42.0	+21 48 02.8	15.69	1.70	2.06	10.963	1.095	2
Be22 414	05 58 25.9	+07 46 11.4	15.76	1.87	2.02	11.020	1.157	3
Be22 643	05 58 26.9	+07 45 26.1	14.31	2.29	2.65	8.369	1.405	3
Be32 16	06 58 06.9	+06 25 56.5	13.61	1.06	...	10.970	0.660	4
Be32 18	06 58 13.8	+06 27 54.9	13.71	1.06	...	11.069	0.640	4
PWM4 RGB1	23 50 57.4	+62 20 03.2	16.19	2.21	...	9.876	1.446	5
PWM4 RGB2	23 50 58.3	+62 19 18.0	16.91	1.99	...	11.185	1.305	5
PWM4 RC1	23 50 53.9	+62 19 07.7	13.015	1.142	...
PWM4 RC2	23 50 53.2	+62 19 33.8	13.087	1.087	...

REFERENCES. — 1 = Kaluzny (1997); 2 = Tosi et al. (1998); 3 = Kaluzny (1994); 4 = Kaluzny & Mazur (1991); 5 = Ortolani et al. (2005)

^a 2MASS (Skrutskie et al. 2006) coordinates and photometry.

spectroscopic data were reduced using the IRAF³ packages as described in Paper I. From the reduced ThAr frames, we measured a spectral resolution of $R = 47,000$ ($\sigma = 3000$) on each of the three detectors, and this value is close to the expected value of $R = 48,000$. Since we did not bin the CCD in the spectral dimension, the data are oversampled with approximately 4.8 pixels per resolution element. The wavelength coverage was from 4000Å to 8500Å. There are gaps in the spectra between the blue and green CCDs ($\sim 5400\text{Å}$ to 5440Å) and between the green and red CCDs ($\sim 7000\text{Å}$ to 7075Å). Furthermore, the free spectral range exceeds the CCD coverage beyond $\sim 6400\text{Å}$.

Exposure times and resulting signal-to-noise ratios (S/N) for the program stars are given in Table 3. (Note that the S/N is given per pixel at 6050Å and that we have 4.8 pixels per resolution element. To obtain S/N ratios per resolution element, multiply our values by 2.19.) Our observing program consisted of relatively short exposures of some stars in order to measure their radial velocities as well as (multiple) longer exposures of other stars to obtain high S/N ratios for detailed

chemical abundance analysis. For the longer exposures, preliminary reduction was performed in real-time in order to estimate the radial velocities. Shorter exposures were taken of four candidate red clump giants (two stars in each of Be 18 and PWM4) and one red giant in PWM4, and the radial velocities were measured during the analysis. Examples of reduced spectra are shown in Figure 11.

2.3. Radial Velocities

Radial velocities were measured by cross-correlating the program stars with radial velocity standards. For 12 November 2006, our radial velocity standard was HD 90861 with a heliocentric radial velocity of 36.3 km s^{-1} (this value was used in Paper I and was taken from the Astronomical Almanac 1999). For 27 December 2006, our radial velocity standard was HD 110885 with a heliocentric radial velocity of -47.89 km s^{-1} (Carney et al. 2003).

The cross-correlation typically involved some 30 orders per star and the dispersion about the mean velocity ranged from 0.1 to 0.7 km s^{-1} . However, we found that on 12 November 2006, the velocity "jumps" by $\sim 2 \text{ km s}^{-1}$ within the consecutive series of spectra taken for Be21-T51. On closer inspection of the data, we found that one of the four spectra obtained has an anomalous radial velocity. The wavelength solution for this spectrum comes from a different ThAr frame than for

³ IRAF (Image Reduction and Analysis Facility) is distributed by the National Optical Astronomy Observatory, which is operated by the Association of Universities for Research in Astronomy, Inc., under cooperative agreement with the National Science Foundation.

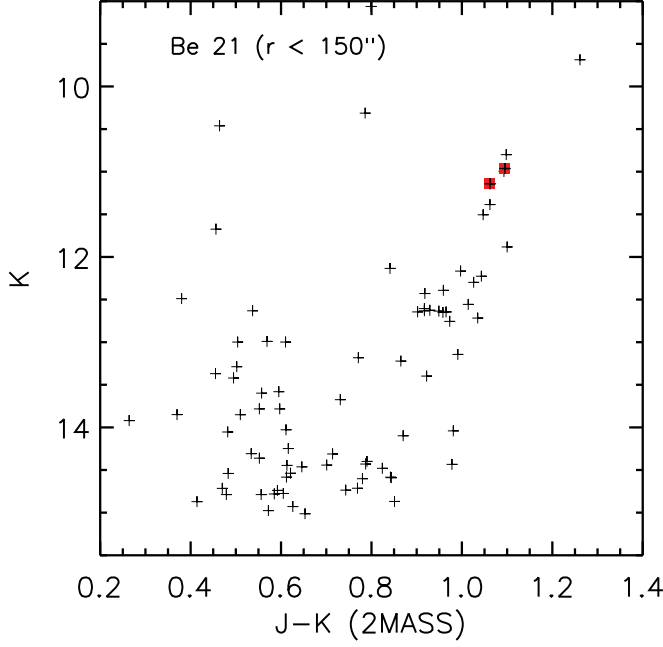


FIG. 4.— Be 21 color-magnitude diagram using the data from 2MASS Skrutskie et al. (2006). We distinguish our program stars by red squares.

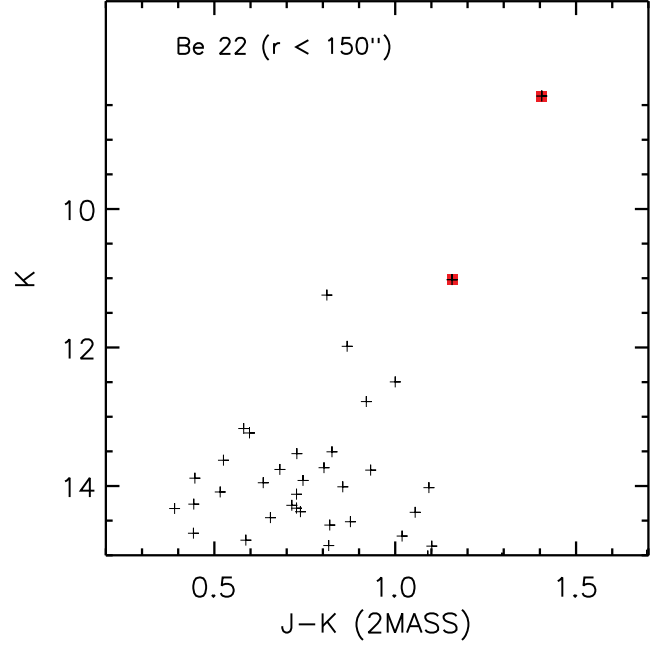


FIG. 6.— Be 22 color-magnitude diagram using the data from 2MASS Skrutskie et al. (2006). We distinguish our program stars by red squares.

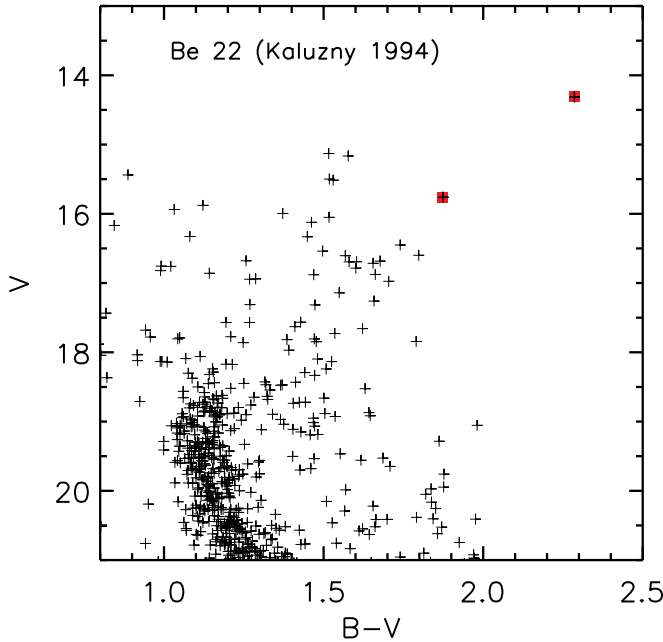


FIG. 5.— Be 22 color-magnitude diagram using the data from Kaluzny (1994). We distinguish our program stars by red squares.

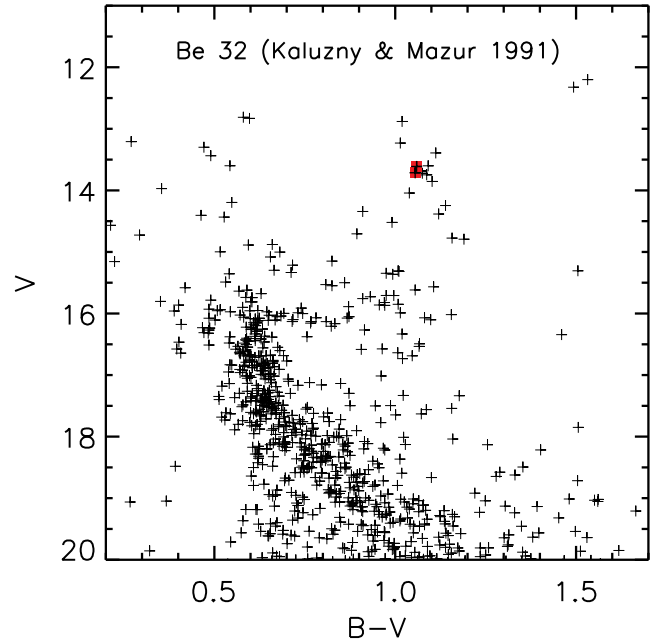


FIG. 7.— Be 32 color-magnitude diagram using the data from Kaluzny & Mazur (1991). We distinguish our program stars by red squares.

the other three spectra. On this observing run, we only took three ThAr spectra, one each at the start and end of the night and only one in the middle of the night. At face value, it would appear that there has been a shift during the course of the night and that the radial velocities on this night probably have a systematic uncertainty of $\sim 2 \text{ km s}^{-1}$. This issue was noted shortly after the November run and more frequent ThAr frames, eight in total, were taken on the December run. For Be21-T51, measurement of the telluric absorption line wavelengths suggests that the three spectra with consistent radial

velocities give the correct value. Another point worth noting is that Be18-1163 was observed on both runs. For this star, we find that the radial velocity from 12 November 2006 is $\sim 1 \text{ km s}^{-1}$ higher than the values obtained from 27 December 2006. This could be explained by either radial velocity variation (and/or jitter – e.g., see Carney et al. 2008 and references therein) or systematic errors in the radial velocity standards. The bottom line is that our radial velocities may be uncertain by $\sim 1 \text{ km s}^{-1}$ between the two observing runs.

For Be18 and PWM4, there are no previous radial velocity

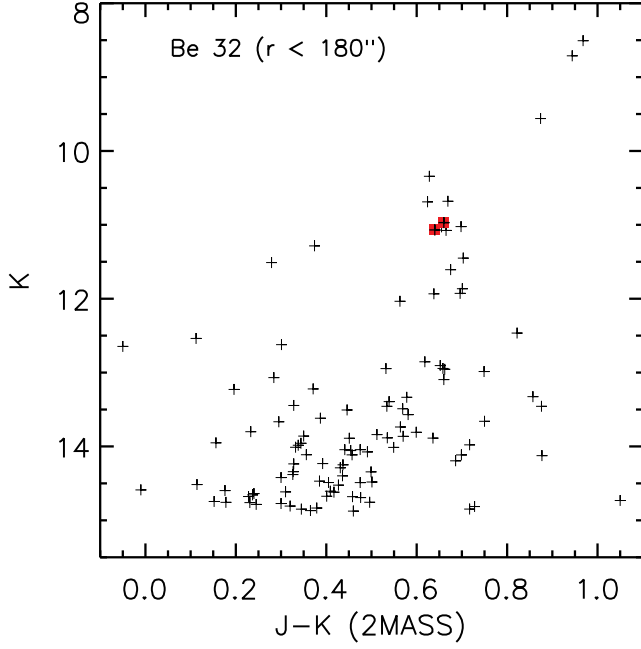


FIG. 8.— Be 32 color-magnitude diagram using the data from 2MASS Skrutskie et al. (2006). We distinguish our program stars by red squares.

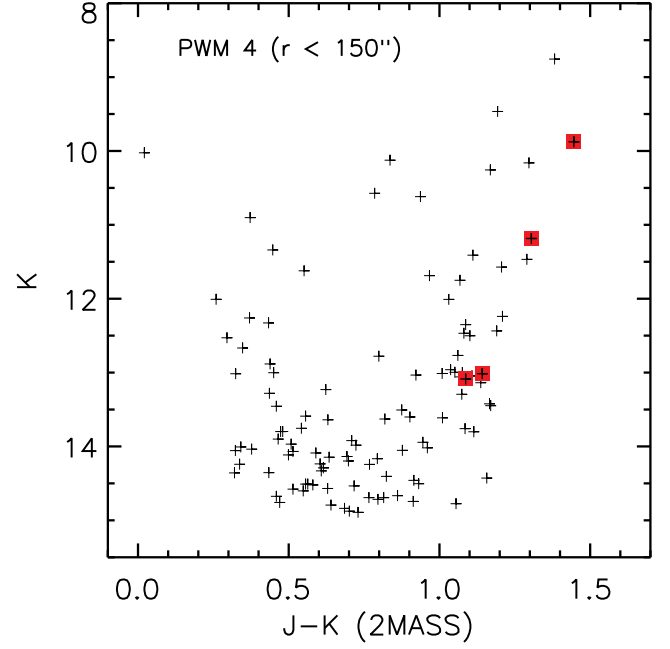


FIG. 10.— PWM 4 color-magnitude diagram using the data from 2MASS Skrutskie et al. (2006). We distinguish our program stars by red squares.

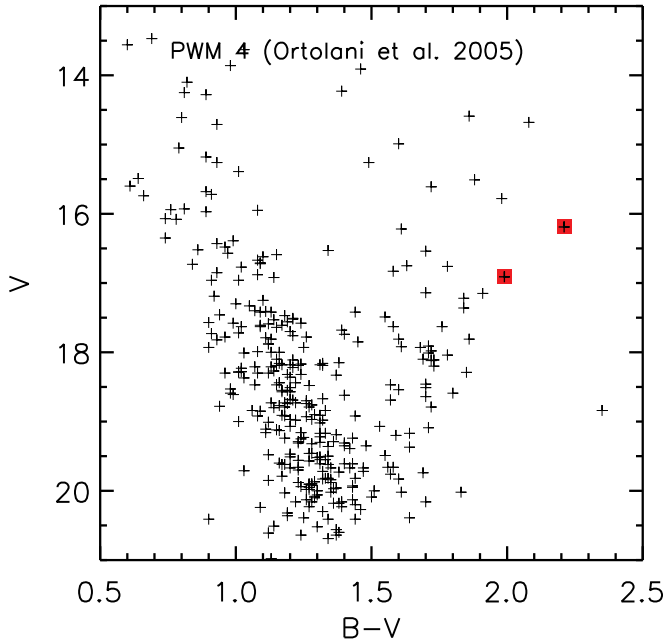


FIG. 9.— PWM 4 color-magnitude diagram using the data from Ortolani et al. (2005). We distinguish our program stars by red squares (the two red clump stars are not included in their photometry).

studies to our knowledge. As noted, Be18-1163 was observed on both runs and there was a 1.0 km s^{-1} radial velocity offset between the two runs. Without knowing which of the two values may be spurious, we include all values for all stars when computing the average cluster radial velocity for Be18 of $-5.5 \pm 1.1 \text{ km s}^{-1}$ ($\sigma = 2.2 \text{ km s}^{-1}$). For PWM4, we find an average cluster radial velocity of $-125.9 \pm 1.0 \text{ km s}^{-1}$ ($\sigma = 2.0 \text{ km s}^{-1}$). For both clusters we studied four stars.

For Be21 T50, our average radial velocity is -1.4 km s^{-1}

TABLE 3
SPECTROSCOPIC OBSERVATIONS

Star	Exposure Time (s)	HJD - 2,450,000	S/N ^a	V_{rad}
Be18-532	600	4052.9209	22	-3.6
Be18-1006	500	4052.9325	20	-8.3
Be18-1163	500	4052.9414	24	-3.1
Be18-1163	2400	4097.7714	48	-4.1
Be18-1163	2401	4097.7998	51	-4.4
Be18-1163	2400	4097.8282	50	-4.4
Be18-1383	1200	4052.9535	48	-6.5
Be18-1383	1800	4052.9717	58	-6.1
Be18-1383	1500	4052.9916	54	-6.1
Be21-T50	2400	4097.9890	53	-1.3
Be21-T50	2401	4098.0174	54	-1.6
Be21-T50	2401	4098.0458	51	-1.2
Be21-T51	2064	4053.0212	53	+0.9
Be21-T51	2400	4053.0535	57	-1.1
Be21-T51	2400	4053.0818	58	-0.9
Be21-T51	600	4053.0998	28	-0.9
Be22-414	2400	4097.8690	51	+93.1
Be22-414	983	4097.8893	31	+93.0
Be22-414	2400	4097.9184	51	+93.4
Be22-414	2533	4097.9487	52	+93.7
Be22-643	1200	4053.1184	72	+90.4
Be22-643	1200	4053.1328	69	+90.4
Be32-16	600	4098.0674	61	+105.9
Be32-16	600	4098.0751	61	+105.9
Be32-16	600	4098.0827	62	+105.8
Be32-18	600	4098.0910	58	+105.1
Be32-18	600	4098.0985	54	+105.1
Be32-18	901	4098.1080	64	+105.1
PWM4-RGB1	2002	4052.7283	42	-125.4
PWM4-RGB1	2700	4052.7631	48	-124.8
PWM4-RGB1	2700	4052.7953	51	-124.8
PWM4-RGB1	2700	4052.8276	51	-124.6
PWM4-RGB2	600	4052.8527	17	-128.8
PWM4-RC1	1800	4052.8709	17	-125.4
PWM4-RC2	1800	4052.8963	16	-124.3

^a Signal-to-noise ratio per pixel near 6050\AA .

($\sigma_{\text{internal}} = 0.2 \text{ km s}^{-1}$) and this value agrees well with the average cluster value of -0.6 km s^{-1} ($\sigma = 2.9 \text{ km s}^{-1}$) from Paper I.

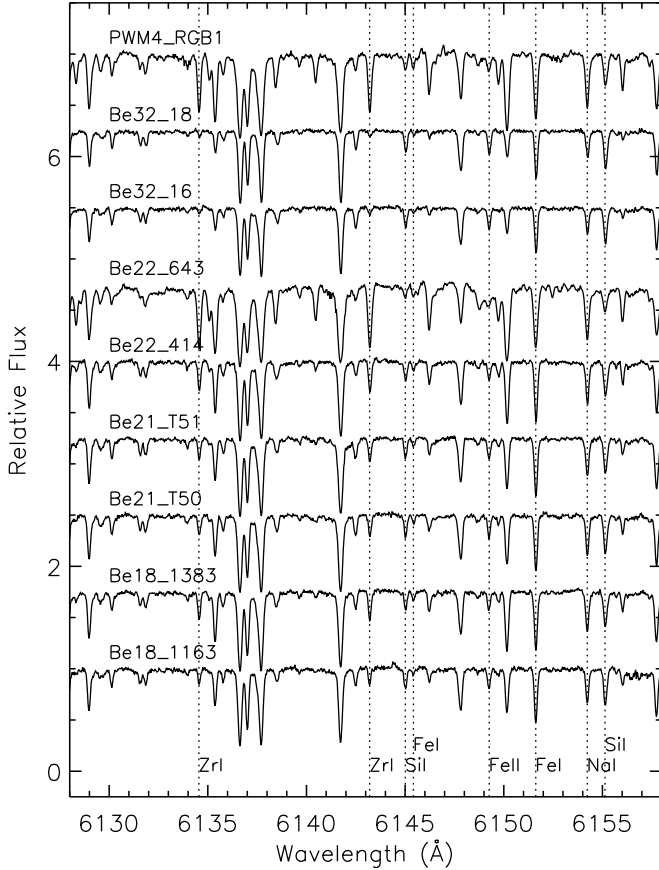


FIG. 11.— Sample region of spectra of the program stars. Lines used in the analysis are marked.

For Be21 T51, our average radial velocity from all four spectra is -0.5 km s^{-1} ($\sigma_{\text{internal}} = 0.9 \text{ km s}^{-1}$). Had we excluded the apparently anomalous $+0.9 \text{ km s}^{-1}$ value, we would have obtained an average value of -1.0 km s^{-1} ($\sigma_{\text{internal}} = 0.1 \text{ km s}^{-1}$). Either value is in good agreement with the value measured for this star in Paper I, $-1.0 \pm 1.0 \text{ km s}^{-1}$. However, as noted in Paper I, our radial velocities for this cluster differ from those of Hill & Pasquini (1999) who obtained $+12.35 \pm 0.6 \text{ km s}^{-1}$ based on four stars.

For Be22, we find an average cluster radial velocity of $+91.9 \pm 1.5 \text{ km s}^{-1}$ ($\sigma_{\text{internal}} = 2.1 \text{ km s}^{-1}$) based on two stars. This value is in fair agreement with the value from Villanova et al. (2005) of $+95.3 \pm 2.0 \text{ km s}^{-1}$ ($\sigma = 2.8 \text{ km s}^{-1}$).

For Be32 18, our average radial velocity of $+105.1 \text{ km s}^{-1}$ is in good agreement with the values from D’Orazi et al. (2006) and Sestito et al. (2006) of $+108.07 \text{ km s}^{-1}$ ($\sigma = 4.12 \text{ km s}^{-1}$) and $+105.5 \text{ km s}^{-1}$, respectively. We find an average cluster radial velocity of $+105.5 \pm 0.4 \text{ km s}^{-1}$ ($\sigma_{\text{internal}} = 0.5 \text{ km s}^{-1}$) based on two stars. Our value is in good agreement with previous studies of this cluster: $+101 \pm 3 \text{ km s}^{-1}$ ($\sigma = 10 \text{ km s}^{-1}$) (Scott et al. 1995); $+106.7$ ($\sigma = 8.5 \text{ km s}^{-1}$) (D’Orazi et al. 2006); $+106.0 \pm 1.4 \text{ km s}^{-1}$ (Sestito et al. 2006); $+105.4 \pm 0.4 \text{ km s}^{-1}$ (Friel et al. 2010).

2.4. Distance Estimations

We determined distances and interstellar reddening for the clusters following the prescription outlined in Paper I. From

the 2MASS color-magnitude diagrams, we estimated the location of the red clump. Carney et al. (2005a) derived a relation between the mean $J-K$ color of the red clump and metallicity. Using our spectroscopic measurement for metallicity, this relation is used to derive the reddening $E(J-K) [= 0.52E(B-V)]$ (Rieke & Lebofsky 1985). The luminosity of the red clump is $M_K \simeq -1.61 \text{ mag}$ and is insensitive to metallicity in the regime $[\text{Fe}/\text{H}] > -1.0$ (Alves 2000). We present our distances and reddening in Table 4. Our distance estimates are, in general, in good agreement with the WEBDA literature values. Such agreement is encouraging given that in some cases, identifying the clump from 2MASS CMDs can be difficult.

3. ELEMENTAL ABUNDANCES

3.1. Stellar Parameters

Stellar parameters are required to conduct a chemical abundance analysis and we obtained the values in the following manner. Following Paper I, initial estimates of T_{eff} come from the infra-red flux method metallicity-dependent color-temperature relations for giant stars by Alonso et al. (1999) and Ramírez & Meléndez (2005). With distances, temperatures, and bolometric corrections, we can calculate $\log g$ values if we assume a mass for the red giants. As in Paper I, we adopt a mass of $1 M_{\odot}$ and note that the surface gravity is not especially sensitive to the assumed value.

These initial estimates for T_{eff} and $\log g$ were then used as starting values for the spectroscopic stellar parameters. Equivalent widths (EW) were measured for a selection of Fe I and Fe II lines using routines in IRAF. We used the same line list as in Paper I. Model atmospheres were computed using the ATLAS9 program (Kurucz 1993). Using the LTE stellar line analysis program MOOG (Sneden 1973), we computed abundances for each line based on the measured EW. (As in Papers I, II, and III, we used the 2002 version of MOOG.) We set the effective temperature, T_{eff} , by requiring that the abundances from Fe I lines showed no trend with lower excitation potential, i.e., excitation equilibrium. The microturbulent velocity, ξ , was determined by ensuring that the abundance from Fe I lines showed no trend with reduced equivalent width, $\log(W_{\lambda}/\lambda)$. We adjusted the surface gravity, $\log g$, until the abundance from Fe I lines agreed with the abundance from Fe II lines, i.e., ionization equilibrium. We also required that the derived metallicity, $[\text{Fe}/\text{H}]$, was within 0.1 dex of the metallicity of the model, $[\text{m}/\text{H}]$, otherwise the model atmosphere was re-computed with the appropriate metallicity. The initial photometric stellar parameters and the final spectroscopic stellar parameters are given in Table 5.

We note that there is good agreement between the photometric and spectroscopic values. Given the large reddening for the program clusters, the infra-red flux method temperatures may be regarded as being less reliable than spectroscopic values. Furthermore, while uncertainties in the distances estimates affect the photometric temperatures, the spectroscopic values are not affected. For PWM4-RGB1, the photometric parameters, using the Ramírez & Meléndez (2005) calibration, differ from our spectroscopic values. Such a discrepancy may be attributed to the uncertainty in the reddening (we obtain $E(B-V) = 0.99$ compared to the WEBDA value of 0.62). With the exception of PWM4, that the two sets of temperatures are in good agreement, in general, probably suggests that the reddening and distance estimates are reasonable.

In practice, we explored discrete values for T_{eff} (every 25 K, i.e., 4525K, 4550K, etc) and $\log g$ (every 0.05 dex, i.e., 1.05

TABLE 4
RED CLUMP DATA

Cluster	$\langle K \rangle$	$\langle J-K \rangle$	[Fe/H]	$(J-K)_0$	$E(J-K)$	$E(B-V)$	$(m-M)_0$	d (kpc)	R_{GC}	$E(B-V)^a$	d^a (kpc)
Berkeley 18	12.21	0.87	-0.4	0.53	0.34	0.66	13.60	5.2	13.10	0.46	5.8
Berkeley 21	12.62	0.93	-0.3	0.55	0.39	0.74	13.98	6.2	14.22	0.76	5.0
Berkeley 22	12.57	0.88	-0.4	0.53	0.35	0.68	13.95	6.2	13.92	0.70	7.7
Berkeley 32	11.02	0.65	-0.3	0.55	0.11	0.20	12.56	3.3	10.97	0.16	3.1
PWM 4	13.02	1.06	-0.3	0.55	0.52	0.99	14.29	7.2	12.91	0.62	7.9

^a Taken from WEBDA.

TABLE 5
ATMOSPHERIC PARAMETERS

Star	T_{eff} Photometric ^a	$\log g$	T_{eff} Photometric ^b	$\log g$	T_{eff}	$\log g$	[m/H] Spectroscopic ^c	ξ_t	[Fe/H]
Be18-1163	4666	2.1	4655	2.1	4500	2.2	-0.5	1.20	-0.46
Be18 1383	4489	1.7	4495	1.7	4400	1.9	-0.5	1.27	-0.41
Be21 T50	4464	1.7	4468	1.7	4625	1.9	-0.3	1.32	-0.26
Be21 T51	4481	1.7	4452	1.6	4500	1.7	-0.3	1.29	-0.35
Be22 414	4340	1.7	4297	1.7	4350	1.7	-0.5	1.18	-0.41
Be22 643	3791	0.6	3752	0.5	3850	0.2	-0.5	1.55	-0.49
Be32 16	4977	2.4	5000	2.4	4875	2.4	-0.3	1.07	-0.39
Be32 18	4962	2.4	5007	2.4	4950	2.7	-0.3	1.46	-0.37
PWM4 RGB1	4368	1.4	3942	1.0	3950	0.5	-0.3	1.28	-0.33

^a Estimates obtained using (i) the photometric data in Table 2, (ii) the distance, reddening, and metallicity from Table 4, and (iii) the Ramírez & Meléndez (2005) IRFM calibration.

^b Estimates obtained using (i) the photometric data in Table 2, (ii) the distance, reddening, and metallicity from Table 4, and (iii) the Alonso et al. (1999) IRFM calibration.

^c Quantities are derived using the spectroscopic methods described in the text.

dex, 1.10 dex, etc). We assumed that excitation equilibrium was satisfied when the slope between $\log \epsilon(\text{Fe I})$ and lower excitation potential was < 0.004 and that ionization equilibrium was satisfied when $|\log \epsilon(\text{Fe I}) - \log \epsilon(\text{Fe II})| < 0.05$ dex. The microturbulent velocity was considered satisfactory when the slope between $\log \epsilon(\text{Fe I})$ and reduced equivalent width was < 0.004 . We iterated until the criteria were simultaneously satisfied. During this process, we estimate that the internal uncertainties are $T_{\text{eff}} \pm 100\text{K}$, $\log g \pm 0.3$ dex, and $\xi_t \pm 0.2$ km s⁻¹.

3.2. Elemental Abundance Analysis

In Paper I, we relied upon spectrum synthesis to measure chemical abundances for individual elements. In that paper, the spectral resolution was $R = 28,000$ and we were concerned that blends might affect the abundances derived from an equivalent width analysis. In this paper, the spectral resolution $R = 47,000$ was sufficiently high that abundance measurements based on EW measurements from our high S/N spectra were regarded to be reliable. Therefore, we measured chemical abundances from spectrum synthesis as well as from equivalent width analysis, when possible, using MOOG in both cases. For both approaches, we took into account the effects of hyperfine splitting and/or isotopic splitting when necessary (e.g., Mn, Co, Rb, Ba, La, and Eu) using the same approach as in Paper I. The line list and solar abundances were the same as in Paper I. (See Table 6 for the atomic data and EW measurements.) In Tables 7 to 11 we present the chemical abundances, $[X/\text{Fe}]$, for the program stars where these values represent the average abundances from EW analysis and from spectrum synthesis. We note that the two approaches

gave quite similar results with an average difference in abundance ratio $\Delta[X/\text{Fe}]$ (EW – Synth) of 0.06 ± 0.01 dex ($\sigma = 0.14$). We did not find any significant global differences for a given line or a given species between the two approaches. (The $[X/\text{Fe}]$ ratios are based on the individual stellar $[\text{Fe}/\text{H}]$ rather than the cluster mean $[\text{Fe}/\text{H}]$.) In Table 12 we show the abundance dependences upon the model parameters for a representative star, Be21 T51, assuming that the errors are symmetric for positive and negative changes.

3.3. Comparison With Literature

Friel et al. (2010) conducted an examination of the various systematic differences between the work by (a) Sestito et al. (2008) and Bragaglia et al. (2008) (SB using their notation), (b) preliminary results from This Study (CY using their notation⁴), and (c) re-analysis by Friel et al. (2010) using the spectra employed by SB and CY. We refer the reader to their careful analysis that takes into account solar abundances, EW measurements, $\log gf$ values and atmospheric parameters. Friel et al. (2010) identify systematic abundance differences between the various studies, but note that “it is difficult to identify the component sources of systematic differences”.

For completeness, we also include a comparison of measured equivalent widths for Be32-18. For 67 lines in common with Bragaglia et al. (2008), we find a mean difference (This Study – Literature) of -4.08 mÅ ($\sigma = 4.71$ mÅ) (see

⁴ The results presented here are very similar to those used in Friel et al. (2010). The average difference in $[X/\text{Fe}]$ is only 0.03 dex ± 0.01 dex ($\sigma = 0.06$ dex). The largest differences were for Na (our $[\text{Na}/\text{Fe}]$ values are lower by 0.14 dex) and Ca (our $[\text{Ca}/\text{Fe}]$ values are lower by 0.18 dex). All other elements are within 0.1 dex.

TABLE 6
EQUIVALENT WIDTHS FOR PROGRAM STARS

Wavelength (Å)	Species	LEP (eV)	$\log gf$	Be18 1163	Be18 1383	Be21 T50	Be21 T51	Be22 414	Be22 643	Be32 16
6300.30	8.0	0.00	-9.72	...	38.7	...	38.9	48.4	114.0	24.9
6363.78	8.0	0.02	-10.19	...	20.8	...	20.3	27.3	83.2	16.3
5688.19	11.0	2.11	-0.42	120.7
6154.23	11.0	2.10	-1.53	60.8	75.0	74.6	73.2	77.8	...	44.3
6160.75	11.0	2.10	-1.23	83.8	97.6	97.9	96.0	103.6	...	68.1
5711.09	12.0	4.35	-1.83	122.5	105.5

REFERENCES. — Note. Table 6 is published in its entirety in the electronic edition of the Astronomical Journal. A portion is shown here for guidance regarding its form and content.

TABLE 7
CHEMICAL ABUNDANCES FOR BERKELEY 18

Species	Abundance	σ	N	Abundance	σ	N
Be18-1163			Be18-1383			
[O/Fe]	0.11	0.07	2
[Na/Fe]	0.10	0.05	2	0.32	0.10	3
[Mg/Fe]	0.25	0.10	4	0.10	0.14	4
[Al/Fe]	0.15	0.04	2	0.22	0.00	2
[Si/Fe]	0.15	0.18	7	0.19	0.04	10
[Ca/Fe]	-0.01	0.18	11	0.25	0.09	6
[Ti/Fe]	0.10	0.17	41	0.27	0.09	30
[Mn/Fe]	-0.27	0.12	3	0.08	0.08	3
[Fe I/H]	-0.47	0.10	46	-0.41	0.12	46
[Fe II/H]	-0.44	0.17	11	-0.41	0.18	8
[Co/Fe]	0.12	0.06	3	0.25	0.08	3
[Ni/Fe]	-0.07	0.15	6	0.04	0.12	6
[Rb/Fe]	-0.31	...	1	-0.15	...	1
[Zr/Fe]	-0.30	0.09	3	-0.11	0.03	3
[Ba/Fe]	0.25	...	1	0.34	...	1
[La/Fe]	0.28	0.07	2	0.39	0.00	2
[Eu/Fe]	0.25	...	1	0.34	...	1

TABLE 8
CHEMICAL ABUNDANCES FOR BERKELEY 21

Species	Abundance	σ	N	Abundance	σ	N
Be21-T50			Be21-T51			
[O/Fe]	0.18	0.04	2
[Na/Fe]	0.39	0.30	3	0.32	0.18	3
[Mg/Fe]	0.17	0.13	4	0.20	0.15	4
[Al/Fe]	0.15	0.00	2	0.19	0.07	2
[Si/Fe]	0.18	0.08	10	0.24	0.08	12
[Ca/Fe]	0.21	0.12	4	0.19	0.11	6
[Ti/Fe]	0.22	0.05	27	0.17	0.04	30
[Mn/Fe]	0.18	0.08	3	0.03	0.13	3
[Fe I/H]	-0.26	0.13	44	-0.35	0.14	31
[Fe II/H]	-0.26	0.16	12	-0.33	0.18	6
[Co/Fe]	0.14	0.08	3	0.15	0.10	3
[Ni/Fe]	0.07	0.15	7	0.06	0.15	6
[Rb/Fe]	0.05	...	1	-0.20	...	1
[Zr/Fe]	-0.05	0.05	3	-0.16	0.06	3
[Ba/Fe]	0.59	...	1	0.58	...	1
[La/Fe]	0.55	0.07	2	0.57	0.07	2
[Eu/Fe]	0.25	...	1	0.36	...	1

TABLE 9
CHEMICAL ABUNDANCES FOR BERKELEY 22

Species	Abundance	σ	N	Abundance	σ	N
Be22-414			Be22-643			
[O/Fe]	0.12	0.04	2	0.21	0.04	2
[Na/Fe]	0.42	0.23	3
[Mg/Fe]	0.16	0.12	3	0.19	0.16	4
[Al/Fe]	0.28	0.00	2	0.49	0.00	2
[Si/Fe]	0.19	0.07	11	0.19	0.17	5
[Ca/Fe]	0.23	0.12	6	0.27	0.27	4
[Ti/Fe]	0.31	0.11	17	0.38	0.19	6
[Mn/Fe]	0.00	0.10	3	-0.45	0.09	3
[Fe I/H]	-0.40	0.11	39	-0.49	0.22	23
[Fe II/H]	-0.44	0.09	10	-0.50	0.33	5
[Co/Fe]	0.25	0.10	3	0.12	0.03	3
[Ni/Fe]	0.06	0.16	6	0.14	0.26	6
[Rb/Fe]	-0.20	...	1	-0.35	...	1
[Zr/Fe]	-0.14	0.08	3
[Ba/Fe]	0.64	...	1	0.57	...	1
[La/Fe]	0.39	0.07	2	0.36	0.00	2
[Eu/Fe]	0.33	...	1	0.19	...	1

TABLE 10
CHEMICAL ABUNDANCES FOR BERKELEY 32

Species	Abundance	σ	N	Abundance	σ	N
Be32-16			Be32-18			
[O/Fe]	0.15	0.04	2	0.30	0.07	2
[Na/Fe]	0.22	0.21	3	0.25	0.28	3
[Mg/Fe]	0.22	0.08	4	0.20	0.08	3
[Al/Fe]	0.16	0.00	2	0.19	0.04	2
[Si/Fe]	0.18	0.10	13	0.22	0.05	13
[Ca/Fe]	0.16	0.20	11	0.14	0.12	12
[Ti/Fe]	0.23	0.07	26	0.29	0.08	30
[Mn/Fe]	-0.13	0.15	3	0.03	0.12	3
[Fe I/H]	-0.38	0.11	59	-0.37	0.10	52
[Fe II/H]	-0.42	0.17	14	-0.36	0.13	16
[Co/Fe]	0.12	0.10	3	0.18	0.15	3
[Ni/Fe]	0.04	0.12	7	0.03	0.12	7
[Rb/Fe]	-0.25	...	1	-0.10	...	1
[Zr/Fe]	-0.11	0.03	3	-0.01	0.03	3
[Ba/Fe]	0.37	...	1	0.20	...	1
[La/Fe]	0.42	0.07	2	0.45	0.07	2
[Eu/Fe]	0.23	...	1	0.38	...	1

Figure 12). While the agreement is reasonable, there is a small systematic difference. (We note that the Bragaglia et al. (2008) spectra are of comparable spectral resolution, $R = 45,000$, and similar S/N.) For Be32-18, uniformly increasing the EWs by 4.0 mÅ, while keeping all stellar parameters unchanged, would increase [Fe/H] by 0.09 dex. We also compare our $\log gf$ values for individual elements with Bragaglia et al. (2008) (see Figure 13). The largest difference is for Si, $\Delta \log gf = 0.12$ dex. For all other elements, the av-

erage differences in $\log gf$ values for a given element are 0.06 dex or smaller.

Next, we compare our abundances [X/H] and [X/Fe] for a given cluster with literature values. In Figure 14 we compare our abundances for stars Be 21 T50 and Be 21 T51 with the three Be 21 stars analyzed by Hill & Pasquini (1999). Our mean metallicity is [Fe/H] = -0.31 while their value is [Fe/H] = -0.54. For the elements in common, our [X/Fe] ratios are on average higher by 0.05 dex ($\sigma = 0.20$ dex). For Ca, there is

TABLE 11
CHEMICAL ABUNDANCES FOR
PWM4

Species	Abundance	σ	N
PWM4-RGB1			
[O/Fe]	0.18	...	2
[Na/Fe]	0.42	0.12	3
[Mg/Fe]	0.23	0.11	4
[Al/Fe]	0.26	0.04	2
[Si/Fe]	0.10	0.05	7
[Ca/Fe]	0.19	0.09	4
[Ti/Fe]	0.14	0.05	6
[Mn/Fe]	-0.28	0.13	3
[Fe I/H]	-0.34	0.15	33
[Fe II/H]	-0.29	0.12	8
[Co/Fe]	0.13	0.06	3
[Ni/Fe]	-0.03	0.11	6
[Rb/Fe]	-0.30	...	1
[Zr/Fe]	0.11	0.06	3
[Ba/Fe]	0.46	...	1
[La/Fe]	0.22	0.07	2
[Eu/Fe]	0.12	...	1

TABLE 12
ABUNDANCE DEPENDENCES ON MODEL PARAMETERS FOR BE
21 T51

Species	$T_{\text{eff}} + 100\text{K}$	$\log g + 0.3 \text{ dex}$	$\xi_t + 0.2 \text{ km s}^{-1}$	Total
[O/H]	-0.01	0.11	-0.01	0.11
[Na/H]	0.09	0.00	-0.05	0.10
[Mg/H]	0.03	0.00	-0.02	0.04
[Al/H]	0.08	-0.01	-0.04	0.09
[Si/H]	-0.04	0.06	-0.04	0.08
[Ca/H]	0.10	-0.02	-0.10	0.14
[Ti/H]	0.17	0.01	-0.10	0.20
[Mn/H]	0.10	0.02	-0.17	0.20
[Fe I/H]	0.06	0.03	-0.09	0.11
[Fe II/H]	-0.09	0.15	-0.07	0.19
[Co/H]	0.05	0.06	-0.06	0.10
[Ni/H]	0.03	0.08	-0.07	0.11
[Rb/H]	0.12	0.00	-0.02	0.12
[Zr/H]	0.21	0.01	-0.03	0.21
[Ba/H]	0.03	0.07	-0.17	0.19
[La/H]	0.02	0.12	-0.06	0.14
[Eu/H]	-0.01	0.12	-0.04	0.13
<hr/>				
[O/Fe]	-0.07	0.08	0.08	0.13
[Na/Fe]	0.03	-0.03	0.04	0.06
[Mg/Fe]	-0.03	-0.03	0.07	0.08
[Al/Fe]	0.02	-0.04	0.05	0.07
[Si/Fe]	-0.10	0.03	0.05	0.12
[Ca/Fe]	0.04	-0.04	-0.01	0.06
[Ti/Fe]	0.11	-0.01	-0.01	0.11
[Mn/Fe]	0.04	-0.01	-0.08	0.09
[Co/Fe]	-0.01	0.03	0.03	0.04
[Ni/Fe]	-0.03	0.05	0.02	0.06
[Rb/Fe]	0.06	-0.03	0.07	0.10
[Zr/Fe]	0.15	-0.01	0.06	0.16
[Ba/Fe]	-0.03	0.05	-0.08	0.10
[La/Fe]	-0.04	0.09	0.03	0.10
[Eu/Fe]	-0.07	0.09	0.05	0.12

a large difference between the two studies, $\Delta[\text{Ca/Fe}] = 0.30$ dex. For all other elements, the maximum difference in $[X/\text{Fe}]$ is 0.11 dex.

In Figure 15 we compare our Be 22 abundances for two stars with the two different stars analyzed by Villanova et al. (2005). Our mean metallicity is $[\text{Fe/H}] = -0.45$ and their value is $[\text{Fe/H}] = -0.32$. For the elements in common, our $[X/\text{Fe}]$ ratios are on average higher by 0.21 dex ($\sigma = 0.12$

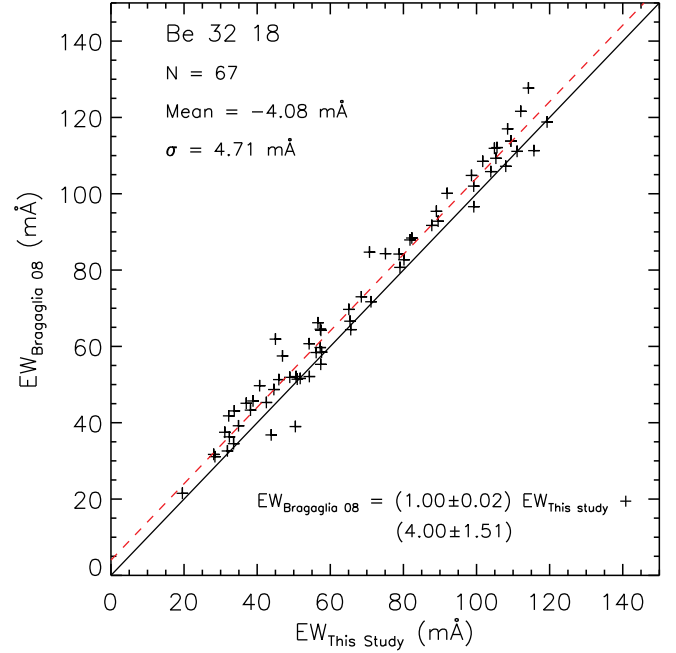


FIG. 12.— Comparison of equivalent width measurements for Be 32 18 between this study and Bragaglia et al. (2008). The one-to-one relation is shown (solid line) along with the linear fit to the data (dashed line).

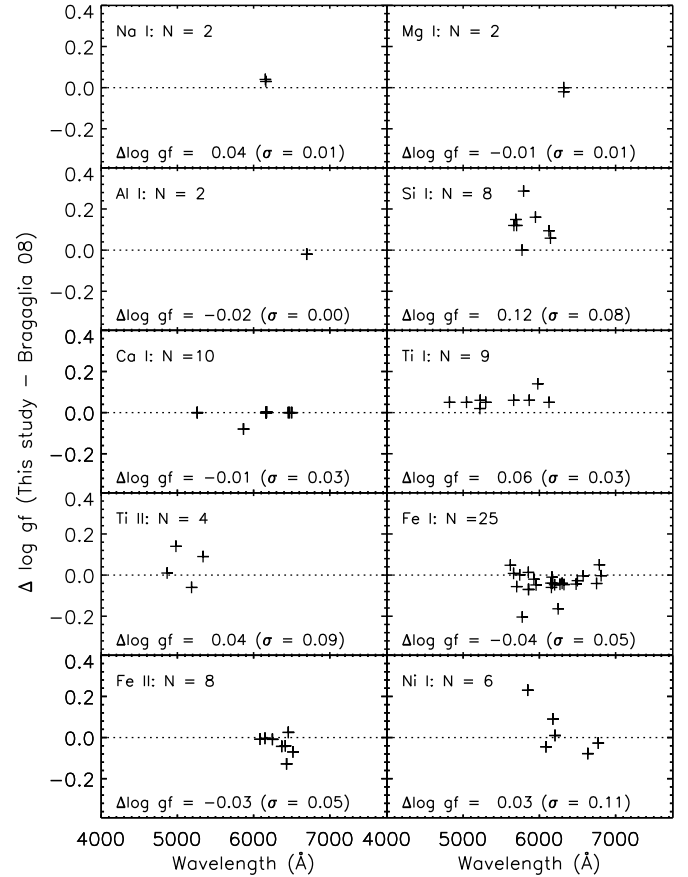


FIG. 13.— Differences in $\log gf$ values for various elements between this study and Bragaglia et al. (2008) versus wavelength.

dex).

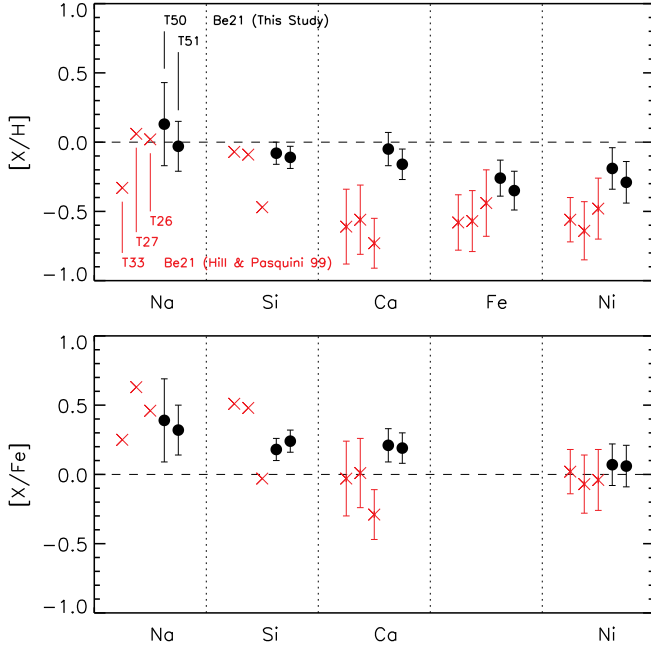


FIG. 14.— Comparison of the abundance ratios $[X/H]$ (upper) and $[X/Fe]$ (lower) in Be 21 between this study (filled circles) and Hill & Pasquini (1999) (crosses). The individual stars are marked and their relative positions are the same in each panel.

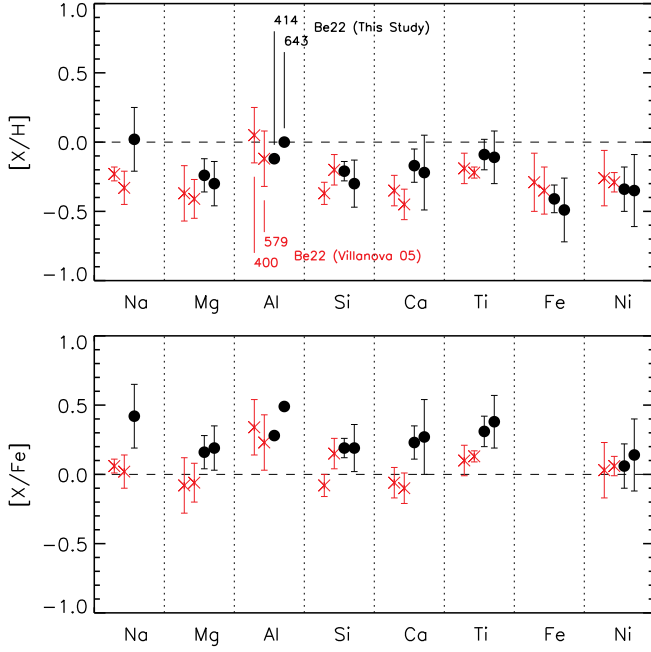


FIG. 15.— Comparison of the abundance ratios $[X/H]$ (upper) and $[X/Fe]$ (lower) in Be 22 between this study (filled circles) and Villanova et al. (2005) (crosses). The individual stars are marked and their relative positions are the same in each panel.

In Figures 16 and 17 we compare our abundances for our two stars in Be32 with the mean cluster values from the analyses of Bragaglia et al. (2008) and Friel et al. (2010). Our mean metallicity, $[Fe/H] = -0.38$, is 0.09 dex lower than Bragaglia et al. (2008), $[Fe/H] = -0.29$. For elements in common, our $[X/Fe]$ ratios are on average higher than those of Bragaglia et al. (2008) by 0.06 dex ($\sigma = 0.07$ dex). Our mean

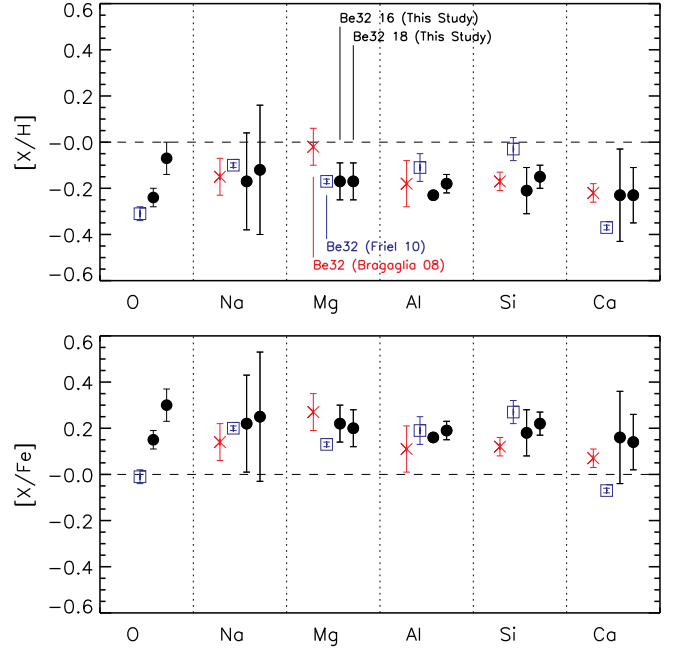


FIG. 16.— Comparison of the abundance ratios $[X/H]$ (upper) and $[X/Fe]$ (lower) for O, Na, Mg, Al, Si, and Ca in Be 32 between the individual stars from study (filled circles) and the mean cluster values from Bragaglia et al. (2008) (crosses) and Friel et al. (2010) (squares).

metallicity, $[Fe/H] = -0.38$, is 0.08 dex lower than Friel et al. (2010), $[Fe/H] = -0.30$. For elements in common, our $[X/Fe]$ ratios are on average higher than those of Friel et al. (2010) by 0.13 dex ($\sigma = 0.15$ dex). This difference is driven primarily by Ti where $\Delta[Ti/Fe] = 0.43$ dex. Such a large abundance difference is of concern, but as noted in Friel et al. (2010) and apparent later in Figure 21, $[Ti/Fe]$ abundances appear to be especially vulnerable to at times large systematic differences between studies. For example, as we shall note in Section 4.4.1, M67 is in common to Friel et al. (2010) and Paper I, and while the two studies obtain very similar metallicities, $\Delta[Fe/H] = -0.01$ dex, a large abundance difference exists for Ti, $\Delta[Ti/Fe] = 0.26$ dex. The origin of these differences is not altogether clear, and does not appear to be due to simple effects of a single source, but is likely driven by a complex combination of factors, such as EWs, stellar parameters, $\log g f$ values, specific lines utilized, reference abundances, analysis techniques, etc.

In Figure 18, we compare our abundances for the star Be32 18 with the analysis of Bragaglia et al. (2008). We derive a metallicity of $[Fe/H] = -0.37$ compared to their value of $[Fe/H] = -0.27$. The elements in common are Na, Mg, Al, Si, Ca, Ti, Ni, Ba, and Fe. For $[X/H]$ we find a mean difference (This Study – Literature) of -0.05 dex ± 0.04 dex ($\sigma = 0.12$ dex). For $[X/Fe]$ we find a mean difference (This Study – Literature) of $+0.05$ dex ± 0.04 dex ($\sigma = 0.13$ dex). We note that, as with the comparison to Friel et al. (2010), the agreement is especially poor for Ti, with $\Delta[Ti/Fe] = 0.27$.

From these comparisons, it is clear that there are systematic differences at the ~ 0.1 dex level between various studies. For some elements, the abundance differences can be as large as 0.4 dex. Such differences should be borne in mind in the comparisons that follow. Of particular interest is that our metallicities are, with the exception of Be 21, lower than the literature values by ~ 0.1 dex which may potentially lead to

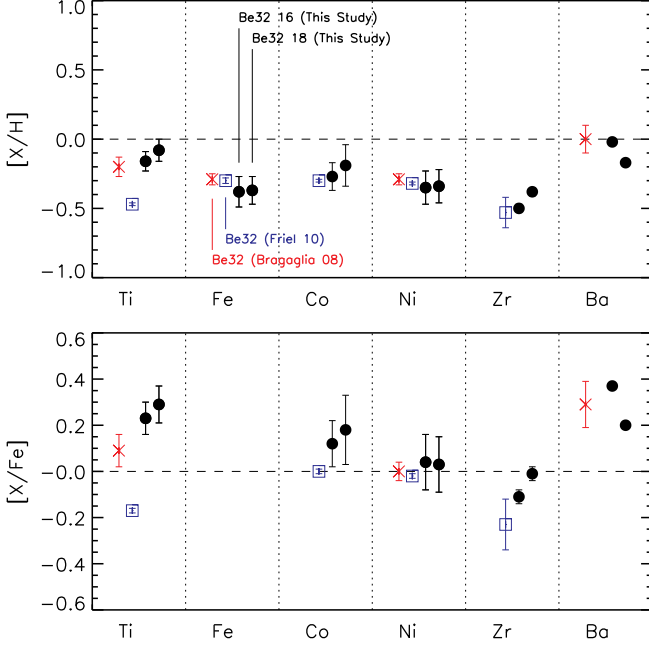


FIG. 17.— Same as Figure 16 but for Ti, Fe, Co, Ni, Zr, and Ba.

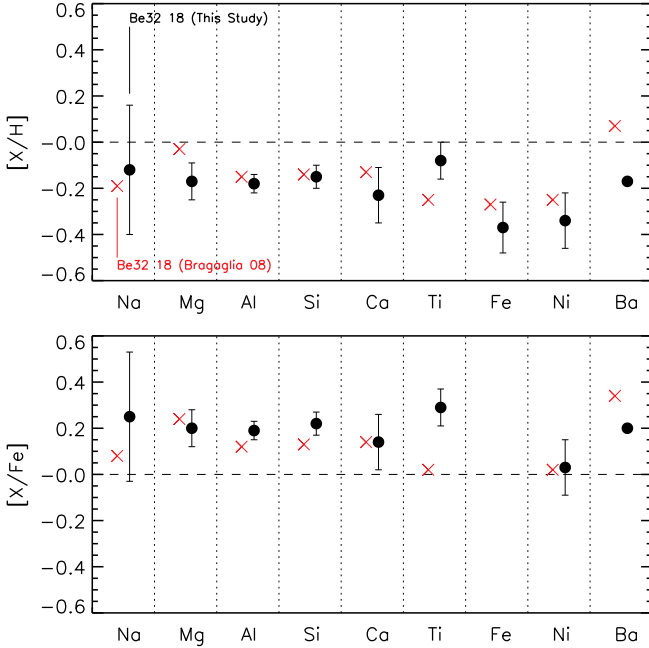


FIG. 18.— Comparison of the abundance ratios $[X/H]$ (upper) and $[X/Fe]$ (lower) in Be 32 18 between this study (filled circles) and Bragaglia et al. (2008) (crosses).

larger $[X/Fe]$ ratios than compared to the literature values. In the subsequent discussion, we will (at times) re-evaluate our conclusions by arbitrarily shifting our metallicities, $[Fe/H]$, by $+0.1$ dex and decreasing our abundance ratios, $[X/Fe]$, by 0.1 dex.

4. DISCUSSION

4.1. Trends With Galactocentric Distance

In Figure 19 we plot the metallicity, $[Fe/H]$, versus Galactocentric distance. This figure includes measurements of

open clusters from this paper (filled circles), Paper I (filled squares), and literature sources (plus signs). (Although membership of Be 31 remains unclear (Friel et al. 2010), we retain this key cluster, $R_{GC} = 12$ kpc, in subsequent figures and discussion.) The compilation of literature data (LTE abundances) and sources used to generate this figure can be found in Table 13. The literature search was not exhaustive. We have not made a critical assessment of the literature sample and note that some of the abundance measurements were based on data that we would regard to have unacceptably low S/N. (In the Appendix A.1, we explore how selections based on S/N may affect the results.) This combined sample consists of some 68 chemical abundance measurements in 49 unique clusters. (We note that Pancino et al. (2010) assembled a compilation of some 57 open clusters. They have more clusters in the solar vicinity but fewer in the outer disk, which is the focus of this series of papers.) One issue is that different authors may adopt independent distances. Therefore, this figure shows the distances from Salaris et al. (2004) (upper panel) as well as the distances from the individual literature sources (lower panel)⁵. In both panels, we join individual clusters with multiple measurements using red lines. That is, in the event that a given cluster has been studied by two or more authors, we treat all studies as independent measurements regardless of the sample size, spectral resolution, and S/N of each study. Following Pancino et al. (2010), rather than averaging multiple measurements into a single value for a given cluster, we show all measurements to provide a “realistic idea of the uncertainties involved in the compilation.” We also measure the linear⁶ fit to the local ($R_{GC} < 13$ kpc) and distant ($R_{GC} > 13$ kpc) samples. The 13 kpc boundary dividing the local and distant clusters was arbitrarily chosen (see Appendix A.2 for a more thorough examination of the division between the inner and outer disk and we also refer the reader to Jacobson 2009 and Jacobson et al. 2011b for further discussion on this issue). As noted previously, the metallicity gradients in the two regions are considerably different. The inner region shows a steeper gradient than in the outer disk. Interestingly, the formal slopes, uncertainties, and dispersion about the linear fit are virtually identical in both panels, that is, these values do not depend upon the distance estimate, Salaris et al. (2004) vs. literature. Our conclusions would not change had we selected a boundary value of 12 kpc or 14 kpc rather than 13 kpc. For completeness, we note that the linear fit includes multiple measurements of a given cluster such that those clusters in effect are given more weight than a cluster with a single measurement. In subsequent figures, we use the literature distance estimates.

The five clusters studied in the present paper lie on, or slightly below, the mean trends. (If we adopt the Salaris et al. (2004) distances, then the two most distant clusters in this paper are more metal-rich than the other three clusters. Al-

⁵ When distances from Salaris et al. (2004) are not available, the values from the individual literature sources are used in the upper panel. Similarly, when distances are not given in the literature sources, the values from Salaris et al. (2004) are employed. The Salaris et al. (2004) distances are based on main sequence fitting and are therefore sensitive to extinction and metallicity. The literature distances come from a variety of methods. As noted in Section 2.4, we use the red clump luminosity. Distances based on this approach are insensitive to metallicity, but identifying the red clump location and extinction affect our results.

⁶ While we determine linear fits to the data throughout the paper, we are not suggesting that this is the correct function to use. Rather, we consider this a first pass to begin to understand the behavior of abundance ratios with distance, age, and/or metallicity, $[Fe/H]$.

TABLE 13
COMPILATION OF (LTE) ABUNDANCE RATIOS FOR OPEN CLUSTERS

Cluster	Source	Age ^a (Gyr)	Distance ^a (kpc)	Age ^b (Gyr)	Distance ^b (kpc)	[Fe/H]	[O/Fe]	[Na/Fe]	[Mg/Fe]	[Al/Fe]	[Si/Fe]
Be 17	Friel10	10.10	11.70	10.06	10.89	-0.10	0.00	0.33	0.12	0.25	0.30
Be 18	This Study	5.69	13.10	5.69	12.09	-0.44	0.11	0.21	0.18	0.19	0.17
Be 20	Sestito08	6.00	16.37	4.05	16.12	-0.30	...	0.17	0.28	0.17	0.05
Be 20	Y05	4.10	16.00	4.05	16.12	-0.49	0.18	0.21	0.24	0.18	0.06
Be 21	This Study	2.18	14.27	2.18	14.27	-0.31	0.18	0.36	0.19	0.17	0.21

REFERENCES. — Bragaglia01 = Bragaglia et al. (2001); Bragaglia08 = Bragaglia et al. (2008); Carraro04 = Carraro et al. (2004); Carrera11 = Carrera & Pancino (2011); Carretta04 = Carretta et al. (2004); Carretta05 = Carretta et al. (2005); Carretta07 = Carretta et al. (2007); de Silva06 = De Silva et al. (2006); de Silva07 = De Silva et al. (2007); Friel10 = Friel et al. (2010); Jacobson et al. (2008, 2009); Friel et al. (2010); Hill99 = Hill & Pasquini (1999); Jacobson11a = Jacobson et al. (2011a); Jacobson11b = Jacobson et al. (2011b); Pancino10 = Pancino et al. (2010); Paulson03 = Paulson et al. (2003); Sestito08 = Sestito et al. (2006, 2007, 2008); Bragaglia et al. (2008); Villanova05 = Villanova et al. (2005); Y05 = Yong et al. (2005)

Note. Table 13 is published in its entirety in the electronic edition of the *Astronomical Journal*. A portion is shown here for guidance regarding its form and content.

^a Ages and distances taken from the individual papers

^b Ages and distances taken from Salaris et al. (2004)

^c Ages and distances taken from Bragaglia & Tosi (2006)

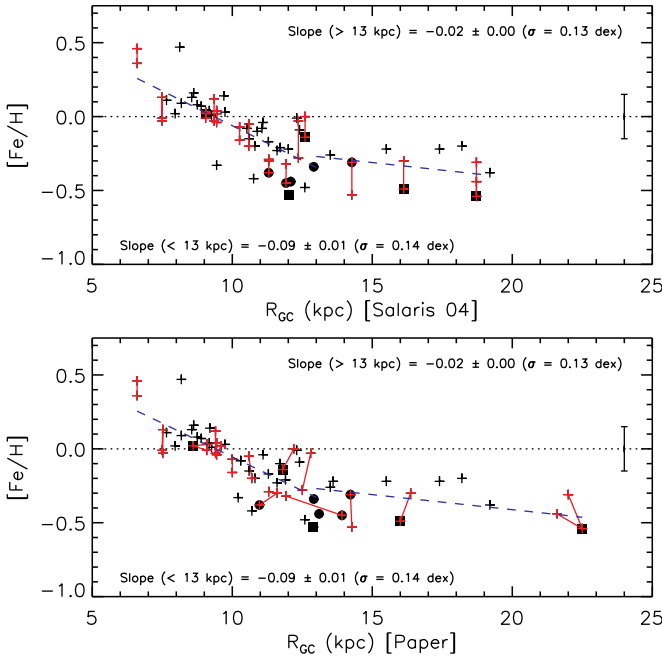


FIG. 19.— [Fe/H] vs. Galactocentric distance. In the upper panel, the distances are taken from Salaris et al. (2004) while in the lower panel, the distances are from the literature papers. The data from this study are filled circles, the Paper I data are filled squares, and the literature data are plus signs. The connected symbols represent multiple measurements of the same cluster. In both panels, we show the linear fit to the data with $R_{GC} < 13$ kpc and $R_{GC} > 13$ kpc. A representative error bar is shown.

though we note that this is not the case for our distance estimates.) Given the inhomogeneous nature of this figure, it is difficult to ascertain whether or not the dispersion about the linear trend represents a real spread in metallicity or systematic offsets between the various studies. Our typical measurement uncertainty for [Fe/H] is 0.15 dex, a value comparable with the dispersion about the linear fit which may indicate that the dispersion about the mean trend may be almost entirely attributable to measurement uncertainties. Indeed, this issue of inhomogeneous comparisons is a recurring theme throughout the rest of the paper. We note that

in this figure, and subsequent figures, no attempt has been made to normalize the abundances onto a common scale. It would be possible to make adjustments for the adopted solar abundances. However, quantifying systematic differences arising from equivalent widths, $\log g f$ values, stellar parameters, model atmospheres, spectrum synthesis codes, and so on would require an independent re-analysis of the entire data set (a substantial, but feasible analysis that should be conducted). Such a re-analysis, which should also include non-LTE and/or 3D effects when possible (e.g., Bergemann & Gehren 2008; Lind et al. 2009), is beyond the scope of the present paper.

Had we shifted our metallicities (i.e., only our measurements in the present paper and in Paper I), [Fe/H], by +0.1 dex, we would have obtained identical slopes for all subsamples considered in Figure 19. For the distant samples, the dispersion about the linear fit would decrease by 0.01 to 0.02 dex depending on the adopted distance scale.

Although we explicitly consider abundance trends with age in the following subsection, we now consider whether the trends and dispersions between metallicity and Galactocentric distance differ when considering open clusters of different age ranges. In Figure 20, we again plot metallicity versus Galactocentric distance, but the sample is split into various age groups: < 2 Gyr, $2 < \text{Age} < 5$, and > 5 Gyr. These bins were arbitrarily chosen to contain roughly equal numbers of clusters and none of our conclusions would change had we changed the age groups by ± 0.5 Gyr. The upper panel of this figure shows the full sample along with the linear fit to the data for the local ($R_{GC} < 13$ kpc) and the distant ($R_{GC} > 13$ kpc) samples. In the lower panels, each of which covers a different age range, we superimpose the linear fit to the complete sample and we re-measure the dispersions about the linear fit for each subsample. The most notable feature of this dissection is that for the local sample, $R_{GC} < 13$ kpc, the scatter about the mean relation is largest for the oldest clusters (> 5 Gyr) and smallest for the youngest clusters (< 2 Gyr). This result would remain unchanged had we (i) shifted our metallicities by +0.1 dex or (ii) excluded the very old (10.2 Gyr) and metal-rich ([Fe/H] = +0.47) cluster NGC 6791 (Carretta et al. 2007).

Clearly, it would be interesting to study whether the tran-

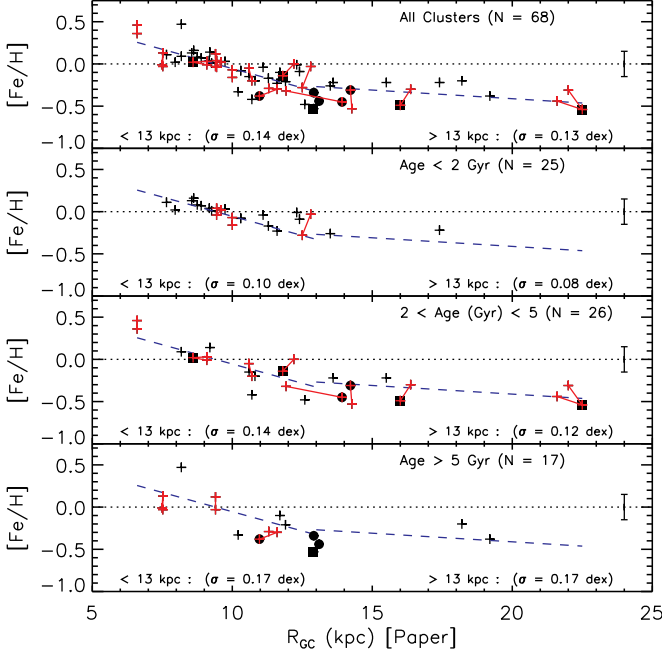


FIG. 20.— $[\text{Fe}/\text{H}]$ vs. Galactocentric distance using the same symbols as in Figure 19. The upper panel shows all stars. The lower panels show stars in various age groups: < 2 Gyr, $2 < \text{Age} < 5$, and > 5 Gyr. The linear fit to the data with $R_{\text{GC}} < 13$ kpc and $R_{\text{GC}} > 13$ kpc is shown in the upper panel. We superimpose these fits to the lower three panels but remeasure the dispersion about the linear fit. A representative error bar is shown.

sition radius between the inner and outer disk changes as a function of age. To this end, Jacobson et al. (2011b) explored this issue and found a suggestion of some variation.

In Figure 21, we plot $[\text{X}/\text{Fe}]$ for the α elements versus Galactocentric distance. In the bottom panel, α represents the direct average of O, Mg, Si, Ca, and Ti. As in previous figures, we compute and plot the fit to the data for $R_{\text{GC}} < 13$ kpc and $R_{\text{GC}} > 13$ kpc. For all elements, there is no statistically significant difference between the gradient for the local and distant samples. While combining the α elements into a single measure may be a convenient way to examine their behavior and to facilitate comparisons with model predictions, we note that the individual elements do not appear to follow identical patterns: $[\text{Ca}/\text{Fe}]$ is roughly solar at all distances, $[\text{Si}/\text{Fe}]$ and $[\text{Mg}/\text{Fe}]$ are uniformly enhanced at all distances, and $[\text{O}/\text{Fe}]$ and $[\text{Ti}/\text{Fe}]$ show considerably higher ratios in the outer disk compared to the inner disk. Thus the behavior of $[\alpha/\text{Fe}]$ would appear to be driven primarily by O and Ti. As noted in Paper I, the outer disk open clusters are probably not members of an older population such as the thick disk (e.g., Bensby et al. 2004) despite some similarities in $[\text{X}/\text{Fe}]$ abundance ratios.

We plot the light elements (Na and Al; Figure 22), the Fe-peak elements (Mn, Co, and Ni; Figure 23), and the neutron-capture elements (Zr, Ba, La, and Eu; Figure 24) versus distance. For the neutron-capture elements discussed here, we note that Zr, Ba, and La are predominantly produced via the s -process while Eu is produced via the r -process (Simmerer et al. 2004). For the neutron-capture elements Zr, Ba, and La, we include the abundance data from D’Orazi et al. (2009) and Maiorca et al. (2011) and distances, when not listed in those references or Salaris et al. (2004), from the Chen et al. (2003) catalogue. We again compute and overplot the linear fit to the local ($R_{\text{GC}} < 13$ kpc) and distant ($R_{\text{GC}} > 13$ kpc) samples.

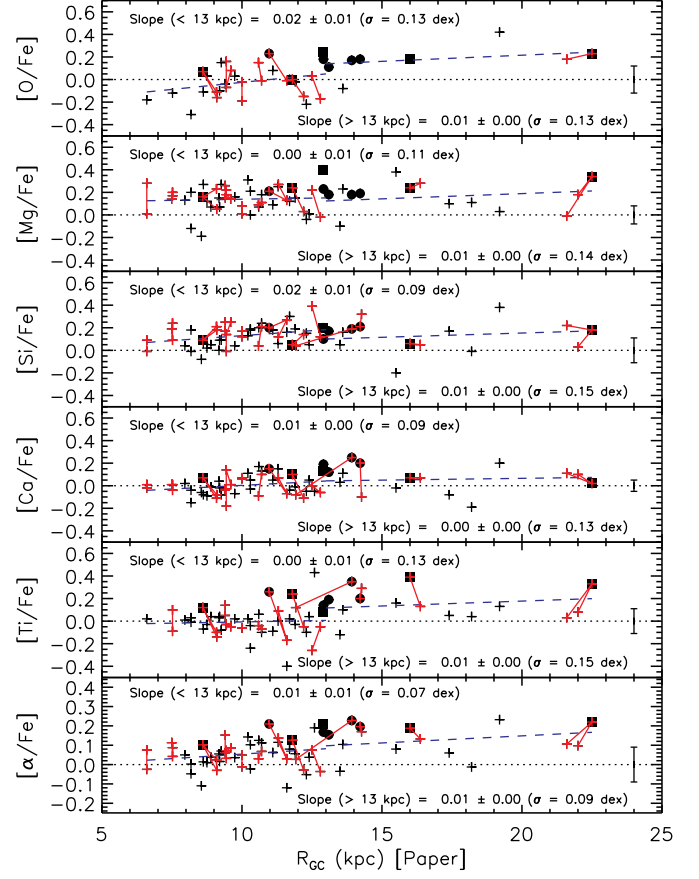


FIG. 21.— Abundance ratios $[\text{X}/\text{Fe}]$ vs. Galactocentric distance for the α elements. Symbols are the same as in Figure 19. In all panels, we show the linear fit to the data with $R_{\text{GC}} < 13$ kpc and $R_{\text{GC}} > 13$ kpc. A representative error bar is shown.

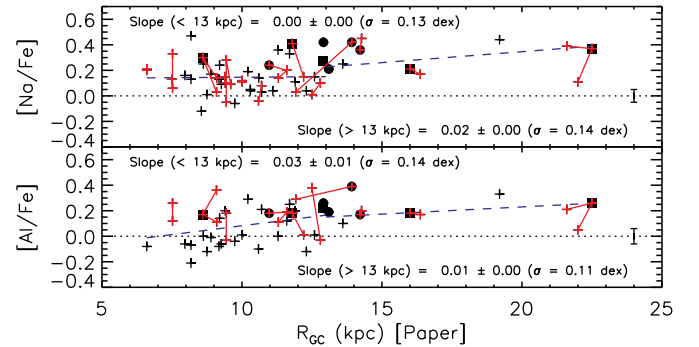


FIG. 22.— Same as Figure 21 but for the light elements $[\text{Na}/\text{Fe}]$ and $[\text{Al}/\text{Fe}]$.

> 13 kpc) samples. While most elements show no significant difference in gradient between the local and distant samples, within the limited data there is a suggestion that Mn, Ba, La, and Eu have different gradients between the local and distant samples.

For all α elements, the gradients are positive (or zero). The maximum value, 0.02 ± 0.01 dex kpc^{-1} , occurs for O and Si in the range $R_{\text{GC}} < 13$ kpc. Therefore, the α elements show only a small trend with increasing R_{GC} . Similarly, Na and Al have positive (or zero) gradients suggesting a slight trend with R_{GC} . The maximum value is 0.03 ± 0.01 dex kpc^{-1} for

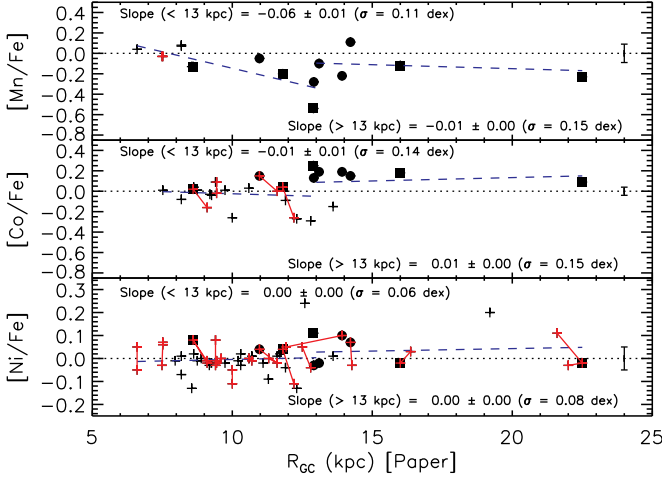


FIG. 23.— Same as Figure 21 but for the Fe-peak elements [Mn/Fe], [Co/Fe], and [Ni/Fe].

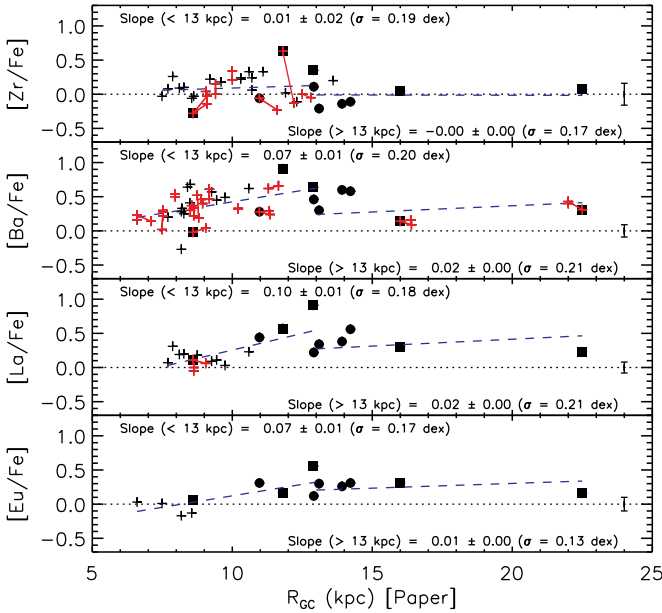


FIG. 24.— Same as Figure 21 but for the neutron-capture elements [Zr/Fe], [Ba/Fe], [La/Fe], and [Eu/Fe].

Al in the range $R_{GC} < 13$ kpc. For the Fe-peak elements Mn, Co, and Ni, the gradients are both positive and negative. The largest value is for Mn in the range $R_{GC} < 13$ kpc, -0.06 ± 0.01 dex kpc $^{-1}$. All other gradients are small. The neutron-capture elements Ba, La, and Eu show large positive gradients in the range $R_{GC} < 13$ kpc. In the outer disk, $R_{GC} > 13$ kpc, their gradients are relatively flat with maximum values of 0.02 dex kpc $^{-1}$. Zr shows no trend with Galactocentric distance.

Another way to compare the abundances between the inner and outer disk is to consider the mean $[X/Fe]$ ratios in the two regions. We again choose a boundary value of $R_{GC} = 13$ kpc between the inner and outer disks. We then measure the mean $[X/Fe]$ ratio as well as the standard error of the mean. By adding the two standard errors of the mean in quadrature and comparing this value to the difference between the two means, we obtain the level of significance. In Table 14, we show for each element the level of significance that the $[X/Fe]$ ratios differ between the inner and outer disk. The elements that

differ at the 3- σ level or higher are O, Na, Al, and Ti. While we note that α is also significant at the 3- σ level, Mg and Si are less than 1- σ and Ca is less than 2- σ . In this table, we also show results when using boundary values of 10 kpc and 15 kpc. For some elements, the level of significance depends strongly upon the adopted boundary.

We now re-consider our results when we arbitrarily increase our $[Fe/H]$ values by 0.1 dex, and therefore decrease our $[X/Fe]$ by 0.1 dex. Recall that this shift in $[Fe/H]$ is motivated by differences between our $[Fe/H]$ values and literature values for clusters in common with the literature. We find that while there remain differences in the mean abundances between the inner and outer disks, the level of significance is lower in some cases; O, Na, Al, Zr, and α are significant at the 2- σ level and Ti is significant at the 4- σ level.

4.2. Trends With Age

Next we explore whether there are any trends between metallicity, $[Fe/H]$, and abundance ratios, $[X/Fe]$, versus age (Figures 25 and 26). In these figures we adopt the ages from Salaris et al. (2004) and individual clusters with multiple measurements are connected with red lines. For the open clusters not included in Salaris et al. (2004), we adopt the ages given in the literature sources (see Table 13 for all ages and references). In all panels of these figures, we compute the linear fit to the data and show the gradient, uncertainty, and dispersion about the linear fit. For all elements there are no significant trends, at the $>3\text{-}\sigma$ level, between abundance and age. The most significant trends we found were for Co, $+0.03 \pm 0.01$ dex/Gyr and Ba, -0.03 ± 0.01 dex/Gyr. (Lines from both elements are affected by hyperfine and/or isotopic splitting and therefore these elements are more likely to be affected by systematic uncertainties than other elements.)

D’Orazi et al. (2009) found that the $[Ba/Fe]$ ratio decreased with increasing age. Maiorca et al. (2011) extended the measurements to additional neutron-capture elements and confirmed the trends between decreasing $[X/Fe]$ with increasing age. We find a similar trend, albeit with a smaller amplitude and significance for Zr and Ba. A likely explanation for this result is that our new measurements of neutron-capture elements in our sample of older clusters fall at higher $[X/Fe]$ ratios than the values in D’Orazi et al. (2009) and Maiorca et al. (2011). For La, we find an opposite trend of increasing $[La/Fe]$ with increasing age.

For some elements, primarily Ni, the dispersion about the linear fit ($\sigma = 0.07$ dex) is comparable to the measurement uncertainty (0.06 dex). We also measure the mean abundance ratio and dispersion for the three age groups used earlier: < 2 Gyr, $2 \text{ Gyr} < \text{Age} < 5$ Gyr, and > 5 Gyr. Given the limited data and inhomogeneous analyses, it would be premature to conclude that the dispersion differs between the various age subsamples, but there are hints for some elements of unusually large, or small, dispersions in various age subsamples. The presence, or absence, of such trends and dispersions would be revealed from a homogeneous analysis.

Again, we reconsider the results when we arbitrarily increase our metallicities by 0.1 dex, and decreasing our $[X/Fe]$ ratios by 0.1 dex. For all elements, the gradients change by ≤ 0.01 dex/Gyr and the dispersion about the linear trends generally decreases by a very small amount.

4.3. Trends With Metallicity

In Figure 27 we plot the abundance ratios $[X/Fe]$ versus metallicity, $[Fe/H]$. In all panels, we plot the linear fit to the

TABLE 14
MEAN $[X/Fe]$ RATIOS, STANDARD ERROR OF THE MEAN, AND LEVEL OF SIGNIFICANCE WHEN COMPARING THE INNER AND OUTER DISK FOR
DIFFERENT BOUNDARY VALUES.

Species	μ	s.e.	μ	s.e.	Significance	μ	s.e.	μ	s.e.	Significance	μ	s.e.	μ	s.e.	Significance
	Inner		Outer			Inner		Outer			Inner		Outer		
	$R_{GC} = 10$ kpc					$R_{GC} = 13$ kpc					$R_{GC} = 15$ kpc				
[O/Fe]	−0.05	0.03	0.06	0.03	2.56	−0.02	0.02	0.17	0.05	3.52	−0.01	0.02	0.25	0.06	4.17
[Na/Fe]	0.14	0.03	0.20	0.02	1.62	0.15	0.02	0.31	0.04	3.97	0.16	0.02	0.28	0.06	2.02
[Mg/Fe]	0.13	0.02	0.15	0.02	0.62	0.14	0.02	0.17	0.04	0.71	0.14	0.02	0.18	0.05	0.93
[Al/Fe]	0.04	0.03	0.16	0.02	2.98	0.09	0.02	0.20	0.03	3.10	0.10	0.02	0.20	0.04	2.20
[Si/Fe]	0.10	0.02	0.15	0.02	1.99	0.13	0.01	0.13	0.04	0.02	0.14	0.01	0.10	0.05	0.70
[Ca/Fe]	−0.03	0.01	0.05	0.02	3.37	0.00	0.01	0.06	0.03	1.66	0.01	0.01	0.03	0.04	0.41
[Ti/Fe]	−0.01	0.01	0.05	0.03	1.82	−0.01	0.02	0.16	0.04	4.00	0.01	0.02	0.15	0.04	2.87
[Mn/Fe]	−0.02	0.03	−0.18	0.06	2.39	−0.11	0.05	−0.11	0.06	0.04	−0.10	0.05	−0.18	0.06	1.03
[Co/Fe]	−0.02	0.03	0.00	0.05	0.55	−0.03	0.03	0.11	0.05	2.21	−0.01	0.03	0.14	0.05	2.71
[Ni/Fe]	−0.01	0.01	0.01	0.01	1.16	0.00	0.01	0.04	0.02	1.67	0.00	0.01	0.05	0.04	1.20
[Zr/Fe]	0.06	0.04	0.10	0.04	0.58	0.09	0.03	−0.02	0.06	1.62	0.08	0.03	0.06	0.01	0.46
[Ba/Fe]	0.32	0.04	0.42	0.05	1.61	0.36	0.03	0.33	0.06	0.43	0.37	0.03	0.26	0.06	1.76
[La/Fe]	0.11	0.03	0.42	0.07	4.19	0.22	0.06	0.36	0.06	1.83	0.25	0.05	0.27	0.04	0.28
[Eu/Fe]	−0.04	0.05	0.28	0.04	5.04	0.11	0.07	0.27	0.03	2.02	0.15	0.06	0.24	0.08	0.86
$[\alpha/Fe]$	0.04	0.01	0.09	0.01	3.12	0.06	0.01	0.13	0.02	3.09	0.06	0.01	0.12	0.03	2.07

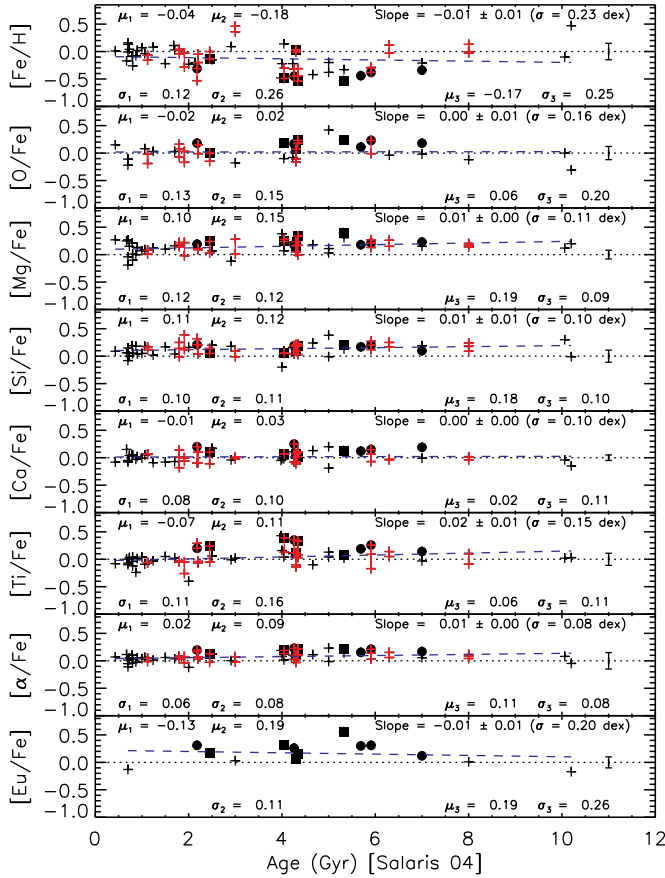


FIG. 25.— Abundance ratios $[Fe/H]$ and $[X/Fe]$ vs. age. The symbols are the same as in Figure 19. The dashed blue line shows the linear fit to the data. In each panel, we also show the mean abundance ratio and dispersion for three age groups: (1) < 2 Gyr, (2) $2 < \text{Age} < 5$, and (3) > 5 Gyr. A representative error bar is included in each panel.

data and show the slope, uncertainty, and dispersion about the linear fit. (As before, the linear fit includes multiple measurements of a given cluster such that those clusters in effect are given more weight than a cluster with a single measurement.) We overplot solar neighborhood thin and thick disk giants from Alves-Brito et al. (2010) as well as solar neighbor-

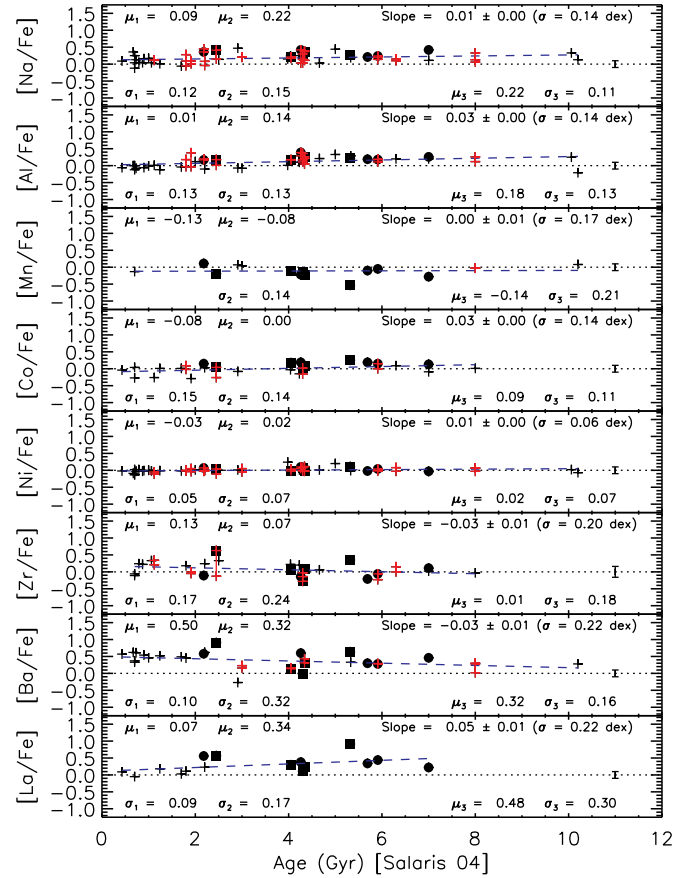


FIG. 26.— Same as Figure 25 but for different elements.

hood giants from Luck & Heiter (2007) which are primarily thin disk objects. The open cluster abundance measurements come almost exclusively from giant stars. Therefore, when comparing the clusters with field stars, we chose to include only giants in order to minimize any systematic abundance differences. For example, comparison of the results for Mg between bulge and local thick disk stars from Fulbright et al. (2007) and Alves-Brito et al. (2010) illustrates the potential systematic differences that may arise when comparing dwarfs

with giants. Additionally, elements such as Na have important non-LTE effects which differ between dwarfs and giants (e.g., Lind et al. 2011). Arguably, any dwarf versus giant abundance discrepancies may be small relative to the systematic differences arising from an inhomogeneous comparison (stellar parameters, atomic data, equivalent widths, solar abundances, model atmospheres, spectrum synthesis software, etc).

For almost all elements, the trends between $[X/Fe]$ versus $[Fe/H]$ for open clusters and field stars are in fair to good agreement. Such agreement would suggest, at face value, that the open clusters, which span a range in ages and distances, have experienced a similar chemical evolution history as did the local field stars which span an unknown (but presumably large) range in age. The obvious discrepancies include Mn and Ba (these elements are affected by hyperfine and/or isotopic splitting) and perhaps O and Na. For Mn, the Luck & Heiter (2007) field giants have higher $[Mn/Fe]$ ratios than do the open clusters. For Ba, the field giants have lower $[Ba/Fe]$ ratios than do the open clusters. As noted, D’Orazi et al. (2009) found a trend of decreasing $[Ba/Fe]$ with increasing age in the open clusters and the lower $[Ba/Fe]$ ratios in field stars could arise if the field stars are systematically older than the open clusters. In the open clusters, $[O/Fe]$ appears lower than field stars of comparable metallicity while $[Na/Fe]$ appears systematically higher than in field stars. While such abundance patterns resemble the O-Na anticorrelation seen in globular clusters (Gratton et al. 2004), the open clusters do not display this abundance pattern (de Silva et al. 2009). The open cluster data are inhomogeneous as are the comparison field stars. Until a systematic and homogeneous analysis is performed upon a sample of open clusters and field stars, we cannot definitively say whether or not the open clusters and field stars have the same, or differing, chemical abundance trends.

In Figure 28, we compare the predicted error in $[X/Fe]$ due to uncertainties in the model parameters (i.e., the values in the fourth column of Table 12) with the dispersion about the linear fit to open clusters in the $[X/Fe]$ versus $[Fe/H]$ plane⁷. For O, Si, Ti, Ni, and Eu, these values are in good agreement suggesting that the dispersion about the linear fit to $[X/Fe]$ versus $[Fe/H]$ can be entirely attributable to the measurement uncertainties. Given the inhomogeneous nature of the open cluster data, this is a slightly surprising result. Notably, $[Ni/Fe]$ and $[\alpha/Fe]$ show dispersions about the linear fit of only 0.07 and 0.06 dex, respectively. For other elements, notably Co, Zr, Ba, and La, the predicted error in $[X/Fe]$ is considerably smaller than the measured dispersion (which reaches values as high as 0.24 dex for Zr and Ba). Such a result would indicate that these elements show a real dispersion amongst the open clusters or that the combined sample is significantly affected by systematic offsets between the various individual studies. For Ba, the lines are generally quite strong and require consideration of hyperfine splitting such that the dispersion will likely be larger than the errors arising solely from uncertainties in the stellar parameters. Furthermore, the trend between $[Ba/Fe]$ and age found by D’Orazi et al. (2009) would introduce additional scatter when considering clusters of all ages in the $[Ba/Fe]$ vs. $[Fe/H]$ plane. Finally, it becomes more dif-

ficult to accurately measure the strengths of strong lines such as Ba and their strength also means that the lines form at shallower optical depths such that the LTE assumption is less reliable.

La may offer a more reliable measure of the *s*-process since there are more lines available to measure including a number of weaker lines. La may show a trend with age (a negative trend according to (Maiorca et al. 2011) and a positive trend according to this study) and therefore inclusion of clusters with a large range of ages may serve to increase the dispersion for $[La/Fe]$ vs. $[Fe/H]$ beyond that expected only from uncertainties in the stellar parameters. Finally, the large dispersions for Zr and Co may be due, in part, to the small number of lines typically used to derive abundances (although some other elements also measured from comparably small numbers of lines show agreement between the predicted and observed abundance dispersions).

We re-examine our results when increasing $[Fe/H]$ by 0.1 dex and decreasing $[X/Fe]$ by 0.1 dex. For the linear fit to the $[X/Fe]$ vs. $[Fe/H]$ data, the slopes increase by an average of 0.08 ± 0.01 dex/dex (i.e., the negative slopes become flatter). Such a result is readily anticipated given that our clusters are amongst the most metal-poor in the combined sample and lowering the $[X/Fe]$ ratios will therefore produce flatter slopes when fitting $[X/Fe]$ vs. $[Fe/H]$. Regarding Ti, our highest $[Ti/Fe]$ ratios are comparable to the upper envelope of field star data and some open cluster literature $[Ti/Fe]$ data lie substantially below the relation defined by the field star data. When adjusting our $[Fe/H]$ and $[X/Fe]$ ratios by 0.1 dex, the dispersion about the linear fit is essentially unchanged and the clusters and field stars remain in good agreement with the exception of the elements already noted, Mn and Ba and perhaps O and Na.

4.4. The Formation and Evolution of the Outer Galactic Disk

4.4.1. Insights from Open Clusters

We now comment on what we can learn about the origin and evolution of the outer disk based on metallicities and chemical abundance ratios in open clusters. The existing data indicate that the outer Galactic disk open clusters ($R_{GC} > 13$ kpc) are uniformly metal-poor, i.e., $[Fe/H] < 0.0$, albeit with metallicities higher than expected based on an extrapolation of the abundance gradient of local open clusters ($R_{GC} < 13$ kpc). Interestingly, we note that the handful of field red giants in the inner Galactic disk (Bensby et al. 2010) are also metal-poor and do not lie on a linear extrapolation of the metallicity gradient based on the solar neighborhood, although these objects have unknown ages and may belong to the thick disk rather than the thin disk. All recent studies of open clusters confirm that the metallicity gradient in the outer disk is flatter than the metallicity gradient near the solar neighborhood. As noted in the introduction, some external galaxies exhibit similar behavior in their outer disks.

We also note that almost all outer disk open clusters have super-solar $[\alpha/Fe]$ and $[Eu/Fe]$ ratios. Such abundance ratios are different from the values found in the more metal-rich open clusters in the solar neighborhood. As already discussed, the $[O/Fe]$, $[Ti/Fe]$, and $[\alpha/Fe]$ ratios differ between the inner and outer disk at the $3\text{-}\sigma$ level or higher (assuming a boundary of 13 kpc). Mg, Si, and Ca do not show significant differences for $[X/Fe]$ between the two regions. Depending on the choice of the boundary value, $[Eu/Fe]$ differs between the inner and

⁷ This approach is only meaningful if we expect the dependence of $[X/Fe]$ versus $[Fe/H]$ to be linear. Inspection of Figure 27 would suggest that the distributions are often non-linear. In addition, we need to be mindful of potential systematic differences between various studies which could serve to increase the observed element abundance dispersion.

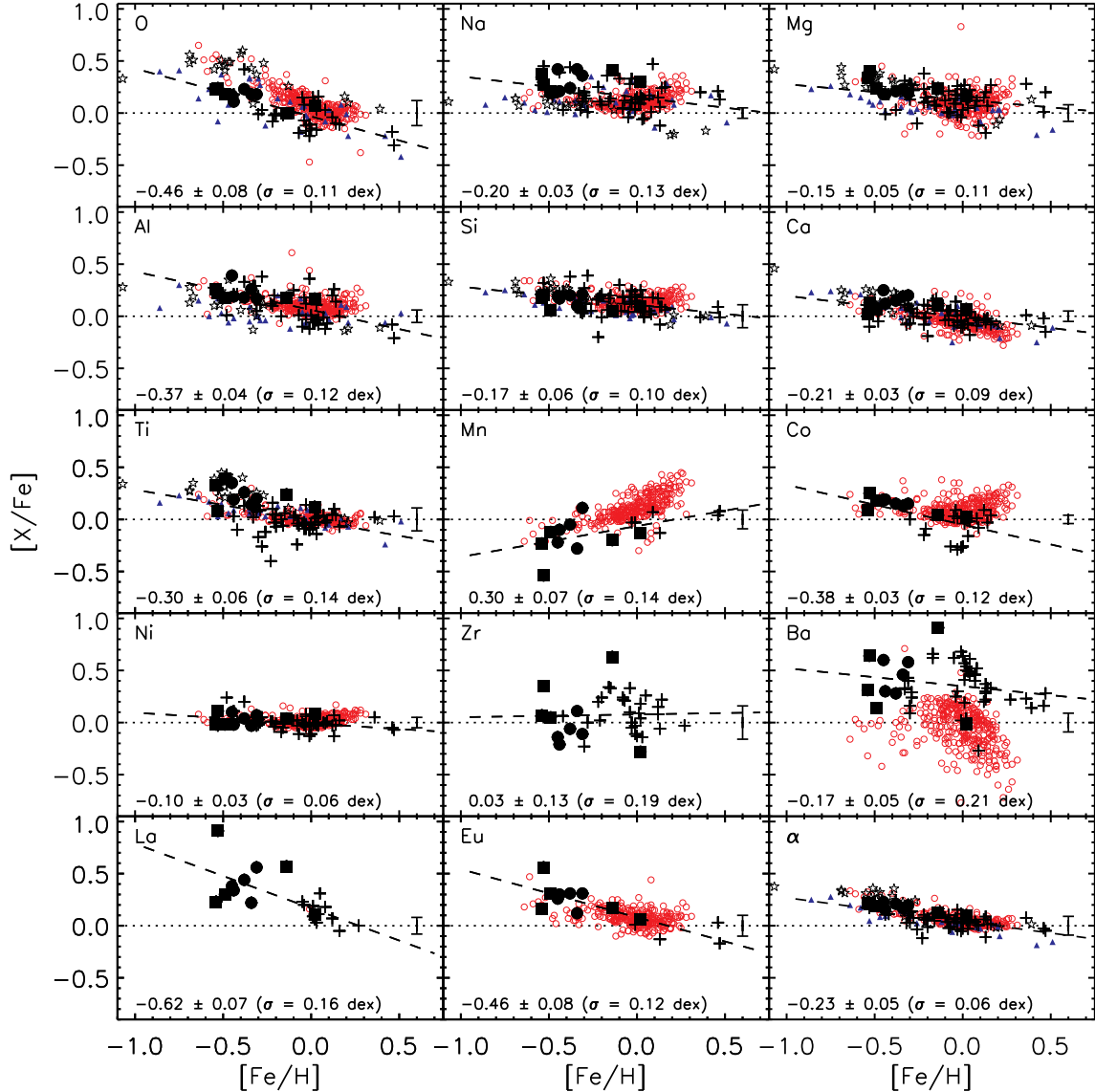


FIG. 27.— $[X/Fe]$ vs. $[Fe/H]$. Literature open clusters (plus signs), clusters from this study (closed black circles), and clusters from Paper I (closed black squares) are plotted. We overplot thin disk (black stars) and thick disk (blue triangles) giants from Alves-Brito et al. (2010) as well as (mainly thin disk) giants from Luck & Heiter (2007) (red open circles). A representative error bar is shown. We plot the linear fit to the open cluster data and write the slope, uncertainty, and dispersion about the slope.

outer regions at the 5.0- σ , 2.0- σ , and 0.9- σ level for 10 kpc, 13 kpc, and 15 kpc, respectively.

As noted, the possibility exists that our $[X/Fe]$ measurements are systematically high. In order to produce $[X/Fe]$ ratios for O, Ti, and Eu that agree within 2- σ between the inner and outer disk would require decreases of 0.2, 0.4, and 0.1 dex for $[O/Fe]$, $[Ti/Fe]$, and $[Eu/Fe]$, respectively. Additional data and a homogeneous re-analysis of the existing data may be necessary to clarify this intriguing situation of enhanced $[\alpha/Fe]$ and $[Eu/Fe]$ ratios in the outer disk.

All s -process elements studied show a significant abundance scatter in the outer disk (and in the solar neighborhood) extending to values as high as $[X/Fe] \simeq +1.0$. Such high abundances of the s -process elements would suggest that asymptotic giant branch stars have played, in some cases, a major role in the chemical evolution of open clusters relative to field stars. Recently, Maiorca et al. (2012) have suggested that the large $[s\text{-element}/Fe]$ ratios seen in young metal-rich

open clusters can be explained by low-mass AGB stars with efficient s -processing.

When comparing the distant open clusters with solar neighborhood field stars at a given metallicity, the abundance ratios $[\alpha/Fe]$ and $[Eu/Fe]$ are in fair agreement. Such similarity in abundance ratios would suggest that in the range of metallicities spanned by both sets of objects, the relative contributions from Type II supernovae (SNe II) and Type Ia supernovae (SNe Ia) are similar. The primary difference is that the chemical enrichment in the outer disk did not yet reach the metallicities of the solar neighborhood. Therefore, the conclusion we drew in Paper I that “high abundances of α -elements indicate rapid star formation, such that Type Ia supernovae did not have sufficient time to evolve and contribute to the chemical evolution” may not be correct since it now appears likely that SNe Ia have made a contribution. Two differences between the present work and that of Paper I are (1) the number of open clusters with chemical abundance measurements has

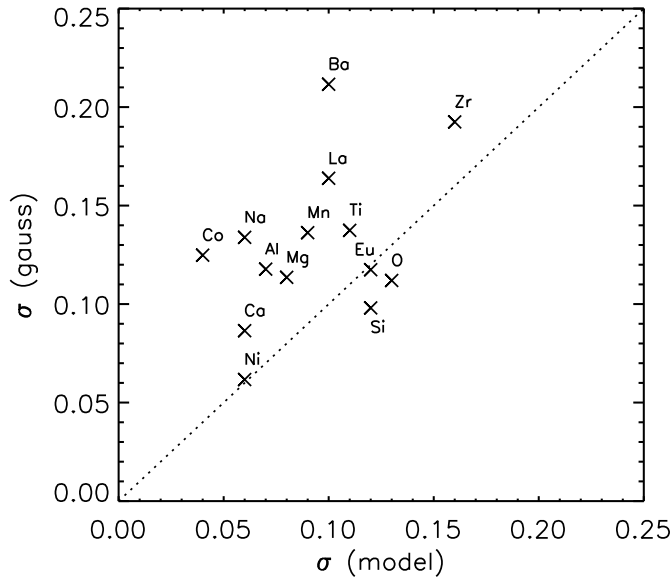


FIG. 28.— Predicted error in $[X/Fe]$ due to uncertainties in the model parameters, σ (model), versus the dispersions about the linear fit to the open cluster data from Figure 27, σ (gauss). The one-to-one relation is shown.

increased considerably and (2) the comparison field stars are all giants which may remove any systematic abundance differences arising from dwarf versus giant comparisons. Clearly it would be of great interest to identify and analyze more metal-rich distant open clusters.

The metal-poor open clusters in the outer disk have super-solar ratios of the α elements and Eu which are primarily produced in massive stars. Since we do not see significant contributions from SNe Ia, we may conclude that the star formation in the outer disk was not prolonged otherwise we would have seen $[\alpha/Fe]$ substantially lower than in field stars of comparable metallicity as found in the more metal-rich stars of the nearby dwarf spheroidal galaxies (Tolstoy et al. 2009). As discussed in Paper I, we would naively expect that the lower density in the outer disk would result in a slower star formation rate relative to the solar neighborhood. In this scenario, we would expect the metallicity gradient to be continuous and that at a given metallicity, the outer disk would have lower $[\alpha/Fe]$ ratios than in the solar neighborhood. As we speculated in Paper I, one possibility for these somewhat unexpected characteristics in the outer disk is that a merger event and/or infall of material triggered a burst of star formation. Such a possibility was reinforced by the results from Paper III in which we found that the young outer disk Cepheids are more metal-poor than the older outer disk open clusters and that some of the Cepheids had enhanced $[\alpha/Fe]$ ratios.

Flat abundance gradients could also be produced by radial mixing (e.g., Roškar et al. 2008; Sánchez-Blázquez et al. 2009; Minchev et al. 2011, 2012) and it is suspected that these processes may play a role in producing the thick disk (e.g., Sellwood & Binney 2002; Haywood 2008; Schönrich & Binney 2009). Jílková et al. (2012) have shown that the Galactic bar and spiral arms may be responsible for moving NGC 6791 from the inner disk to its current location, although they regard the probability to be very low. While it may be possible for strongly bound clusters to survive the migration, to our knowledge no detailed study has yet been performed.

Finally, we caution that any interpretation of the abundance

ratios from compilations needs to acknowledge that the open clusters were studied by various authors who adopt different analysis techniques. We also note that for M67, a recent study by Öneħag et al. (2011) showed that this cluster has a metallicity $[Fe/H] = +0.02$ and abundance ratios $[X/Fe]$ within 0.03 dex of the solar values. Their strictly differential analysis of one dwarf star with almost identical stellar parameters to the Sun, a so-called solar twin, enabled very high precision. For comparison, in Paper I our analysis of M67 giants found near solar metallicity, $[Fe/H] = 0.02$, but $[X/Fe]$ ratios that differed from the solar value. The elements with $[X/Fe] \geq 0.1$ dex are Na, Mg, Al, Ti, and La and those with $[X/Fe] \leq -0.1$ dex are Mn and Zr. Table 13 includes an additional study of M67 giants by Friel & Jacobson (e.g., Friel et al. 2005; Jacobson et al. 2008, 2009; Friel et al. 2010; Jacobson et al. 2011a) that also found $[X/Fe]$ ratios that differ from solar by 0.1 dex or more, including Ti for which they find $[Ti/Fe] \leq -0.1$. Therefore, the Öneħag et al. (2011) results serve to highlight any systematic abundance offsets between studies that have included this target. We also note that our Paper I analysis included the bright giant Arcturus such that future studies can identify abundance offsets. Additionally, membership has not been unambiguously determined for some key clusters, e.g., Be 31 (Friel et al. 2010).

4.4.2. Insights from Field Red Giant Stars

Chemical abundance measurements exist for a number of field stars beyond $R_{GC} = 10$ kpc. These objects include Cepheids (which we shall discuss in Sec 4.4.3), young OB stars (Daflon & Cunha 2004) as well as field red giants (Carney et al. 2005b; Bensby et al. 2011) which we assume to have ages comparable to the open clusters. We focus here on the field red giants and compare the abundances obtained in these objects to the open cluster data. The main issue we seek to address here is whether the field star population is chemically distinct from the open clusters. While we do not necessarily expect any chemical differences between the two samples, it is important to conduct the comparison.

Before continuing, we caution that outer disk field red giants may be affected by selection biases. Stars beyond say $R_{GC} = 10$ kpc are likely chosen to lie well above, or below, the Galactic plane to avoid reddening. We speculate that such selection criteria may therefore give strong weight towards thick disk stars over thin disk stars (although see Bensby et al. 2011 for a discussion of the scale length and scale height of the thick disk).

In Figure 29, we plot $[Fe/H]$, $[Mg/Fe]$, $[Si/Fe]$, and $[Ti/Fe]$ vs. R_{GC} (left panels) for open clusters and field stars (Carney et al. 2005b; Bensby et al. 2011). In these panels, we plot the linear fit to the local and distant open cluster samples. The first notable aspect from this figure is that the field star samples from Carney et al. (2005b) and Bensby et al. (2011) do not extend to the same large distances as do the open clusters. The second point we highlight is that the field stars are, on average, more metal-poor than the open clusters at the same distances. For open clusters with $10 \text{ kpc} \leq R_{GC} \leq 12 \text{ kpc}$ the mean metallicity is $[Fe/H] = -0.20$ and the dispersion is $\sigma[Fe/H] = 0.11$ dex. For the field stars in the same range of Galactocentric distances, we find a mean metallicity of $[Fe/H] = -0.48$ and dispersion of $\sigma[Fe/H] = 0.13$ dex. It is not obvious why the metallicity difference exists between the open clusters and field stars at the same Galactocentric distances. Systematic offsets between the various studies at

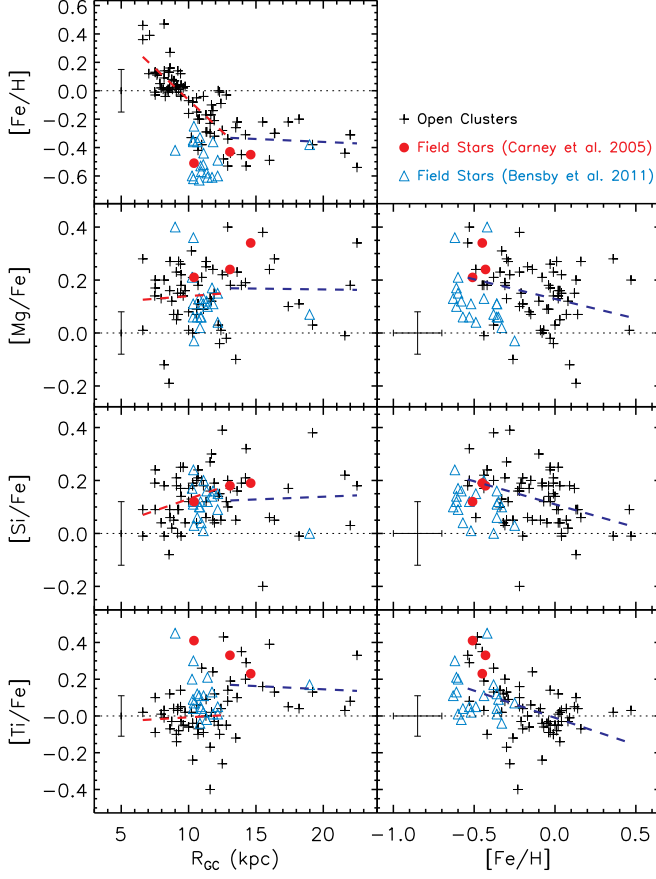


FIG. 29.— $[\text{Fe}/\text{H}]$, $[\text{Mg}/\text{Fe}]$, $[\text{Si}/\text{Fe}]$, and $[\text{Ti}/\text{Fe}]$ vs. R_{GC} (left panels) and $[\text{Mg}/\text{Fe}]$, $[\text{Si}/\text{Fe}]$, and $[\text{Ti}/\text{Fe}]$ vs. $[\text{Fe}/\text{H}]$ (right panels) for open clusters (plus signs), field stars from Carney et al. (2005b) (filled red circles), and field stars from Bensby et al. (2011) (blue open triangles). In the left panels, we fit the local ($R_{\text{GC}} < 13$ kpc) and distant ($R_{\text{GC}} > 13$ kpc) open clusters and in the right panels, we fit the open cluster data. Representative error bars are included in each panel.

the ~ 0.3 dex level would be necessary to explain these differences or the field stars could be thick disk objects. Alternatively, it may be that the difference in metallicity between the samples are due to selection biases in the field stars. Raising our open cluster metallicities by 0.1 dex would only serve to increase the discrepancy in $[\text{Fe}/\text{H}]$ between open clusters and field stars. The third point we note is that the dispersion in $[\text{Fe}/\text{H}]$ for the Bensby et al. (2011) data (0.13 dex) is comparable to the dispersion in $[\text{Fe}/\text{H}]$ for the open clusters at similar distances (0.11 dex).

We now compare the distributions of $[\text{Mg}/\text{Fe}]$, $[\text{Si}/\text{Fe}]$, and $[\text{Ti}/\text{Fe}]$ vs. R_{GC} for the field stars and open clusters. Taking objects in the range $10 \text{ kpc} \leq R_{\text{GC}} \leq 12 \text{ kpc}$, we find mean values and dispersions of $[\text{Mg}/\text{Fe}] = 0.15$ ($\sigma = 0.09$) for the open clusters and $[\text{Mg}/\text{Fe}] = 0.11$ ($\sigma = 0.09$) for the field stars. For Si, we find mean values and dispersions of $[\text{Si}/\text{Fe}] = 0.16$ ($\sigma = 0.08$) and $[\text{Si}/\text{Fe}] = 0.12$ ($\sigma = 0.06$) for the open clusters and field stars, respectively. For Ti, we find mean values and dispersions of $[\text{Ti}/\text{Fe}] = -0.03$ ($\sigma = 0.15$) and $[\text{Ti}/\text{Fe}] = 0.09$ ($\sigma = 0.09$) for the open clusters and field stars, respectively. While $[\text{X}/\text{Fe}]$ is in very good agreement between open clusters and field stars in the same range of Galactocentric distances, there are very few field stars beyond $R_{\text{GC}} = 13$ kpc with chemical abundance measurements. There is a clear need to study more distant field stars to understand the chemical properties of the

outer Galactic disk. Had we decreased our $[\text{X}/\text{Fe}]$ ratios by 0.1 dex, arguably the agreement in $[\text{X}/\text{Fe}]$ between field red giants and open clusters would remain satisfactory.

In the right panels of Figure 29, we compare $[\text{X}/\text{Fe}]$ vs. $[\text{Fe}/\text{H}]$ between the field stars and the open clusters. It seems that the field stars have lower $[\text{X}/\text{Fe}]$ ratios, on average, than do the open clusters at the same metallicity. Within the limited samples and bearing in mind the measurement uncertainties and possible systematic offsets, the field stars and open clusters seem to follow the same trends between abundance ratios $[\text{Fe}/\text{H}]$ and $[\text{X}/\text{Fe}]$ vs. R_{GC} and between $[\text{X}/\text{Fe}]$ vs. $[\text{Fe}/\text{H}]$. Therefore, our tentative conclusion is that the interpretation of the outer Galactic disk does not depend significantly upon whether we use open clusters or field stars although we remind the reader that selection biases for the field stars may give much stronger weight to thick disk objects.

4.4.3. Insights from Cepheids

Studies of the chemical abundances of Cepheids provide a complementary view on the radial abundance gradients in the disk. With their high masses and short lifetimes, the Cepheids likely reflect the present-day chemical composition of the disk. A number of studies within the last decade have explored the radial abundance gradients as traced by Cepheids (e.g., Andrievsky et al. 2002b,a,c, 2004; Lemasle et al. 2008; Luck et al. 2003, 2011; Luck & Lambert 2011; Pedicelli et al. 2009; Yong et al. 2006).

While the time variation in radial abundance gradients can be obtained by comparing the younger and older open clusters, we note that the sample sizes are modest (e.g., our compilation has 24 and 43 clusters with ages below 1 Gyr and above 2.5 Gyr, respectively, and of the 24 clusters younger than 1 Gyr, only 3 lie beyond $R_{\text{GC}} = 12$ kpc and none beyond 14 kpc). Instead, comparison between Cepheids and old open clusters offers a larger sample (e.g., Luck & Lambert 2011 have a homogeneous sample of 339 Cepheids including 40 and 15 objects beyond 12 kpc and 14 kpc, respectively) and arguably a more robust measure of the time variation of radial abundance gradients. (We note that planetary nebulae also offer important insights into the chemical evolution of the Galactic disk, although their distant uncertainties are large relative to those of open clusters and Cepheids. We refer the interested reader to Maciel et al. (2003), Costa et al. (2004), and Maciel & Costa (2009) and references therein.)

One concern is that there may be large systematic differences between the abundances obtained from open cluster red giants and those from Cepheids. Indeed, caution must be exercised when directly comparing abundances between open clusters and Cepheids. However, abundance gradients basically represent a differential abundance comparison between similar stars but at different Galactocentric distances. If each sample (open cluster giants or Cepheids) is analyzed uniformly, then the systematic errors in the analysis of a particular type of star should largely cancel thereby enabling the radial gradient comparisons we seek to conduct.

In Figure 30, we plot $[\text{Fe}/\text{H}]$ vs. R_{GC} for the open clusters and for the Cepheids from Luck & Lambert (2011). This figure enables us to address whether the older open clusters have a different $[\text{Fe}/\text{H}]$ radial gradient than the young Cepheids. Therefore, we only plot open clusters with ages greater than 2.5 Gyr. Additionally, we divide the open clusters and Cepheids into a local ($R_{\text{GC}} < 13$ kpc) and distant ($R_{\text{GC}} > 13$ kpc) samples. We measure the linear fit to all subsamples and write the slope, uncertainty, and dispersion

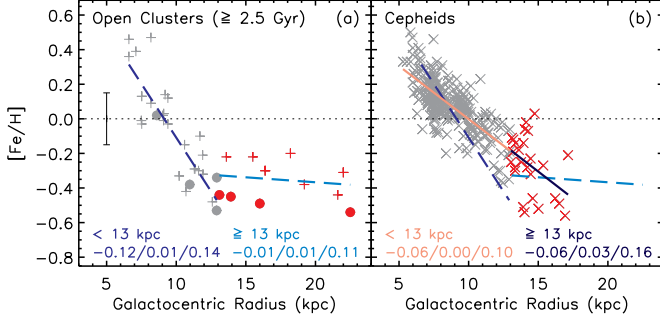


FIG. 30.— [Fe/H] vs. R_{GC} for the older open clusters (age ≥ 2.5 Gyr; left panel) and Cepheids (right panel). Data with $R_{GC} < 13$ kpc are in grey while data with $R_{GC} > 13$ kpc are in red. Open clusters from our work are shown as filled circles while the Cepheid data are from Luck & Lambert (2011). We determine the linear fit, uncertainty, and dispersion about the linear fit to the local and distant open clusters and Cepheids. For the Cepheid data, we superimpose the linear fits to the open cluster data.

about the linear fit in Figure 30. As noted in previous studies of Cepheids, there is no sudden change in gradient between [Fe/H] and R_{GC} . In contrast to the open clusters, the Cepheids decrease smoothly in metallicity with increasing distance. The same result would apply had we overplotted our Cepheid data from Paper III. Since 21 of those 24 stars were studied by Luck & Lambert (2011), for convenience we rely only upon their data to ensure a homogeneous sample. Next, we note that for the inner samples, the older open clusters show a much steeper abundance gradient (-0.12 ± 0.01 dex/kpc) than the younger Cepheids (-0.06 ± 0.00 dex/kpc).

In Figure 31, we plot [Mg/H] and [Mg/Fe] vs. Galactocentric distance as well as [Mg/Fe] vs. [Fe/H] for the open cluster and Cepheid samples. We again determine the linear fit to the local and distant samples. For the local sample ($R_{GC} < 13$ kpc), the older open clusters show a steeper gradient for [Mg/H] compared to the younger Cepheids, a result also seen for [Fe/H]. This analysis was repeated for each element and in Figure 32, we compare the gradients for [X/H] vs. R_{GC} between open clusters and Cepheids with $R_{GC} < 13$ kpc. For the open clusters, we consider only clusters with ages ≥ 2.5 Gyr (upper panel) and ≥ 1.5 Gyr (middle panel). For both cases, we find that the gradient for [X/Fe] vs. R_{GC} is always shallower for the Cepheids compared to the older open clusters, with the exception of La. Such a time variation in radial abundance gradient is in the same sense as predicted by chemical evolution models (e.g., Hou et al. 2000; Fu et al. 2009; Pilkington et al. 2012) and is believed to be due to the “inside-out” formation of the disk.

As a further comparison, we measured the radial abundance gradients in the youngest open clusters. The 24 open clusters with ages ≤ 1.0 Gyr all lie within $R_{GC} = 13$ kpc. The radial abundance gradient for [Fe/H] is -0.05 ± 0.01 dex/kpc, a value in excellent agreement with the local Cepheids (-0.06 ± 0.00 dex/kpc). In the lower panel of Figure 32, we compare the radial abundance gradients, [X/H], for the young Cepheids and youngest open clusters (we only show data for those elements for which there were four or more clusters). The excellent agreement in radial abundance gradients for the two sets of young objects validates our expectation that radial gradients represent a differential comparison within which the systematic errors cancel.

One issue we can address with these data is whether the outer disk open clusters ($R_{GC} > 13$ kpc) share the same [X/H] abundance gradient as the inner disk open clusters ($R_{GC} < 13$

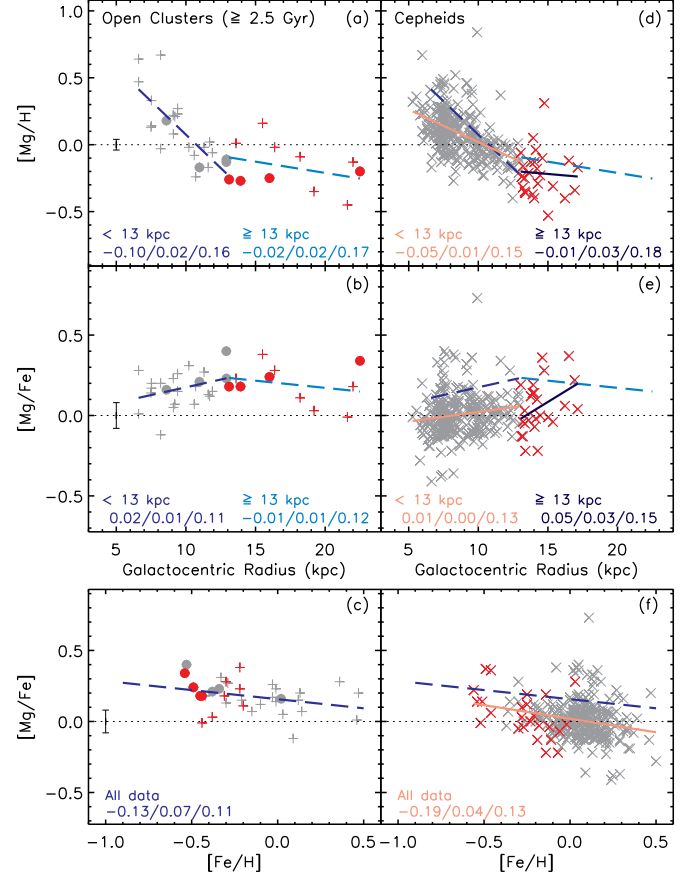


FIG. 31.— [Mg/H] and [Mg/Fe] vs. R_{GC} and [Fe/H] for the open clusters (left panel) and Cepheids (right panel). Data with $R_{GC} < 13$ kpc are in grey while data with $R_{GC} > 13$ kpc are in red. Open clusters from our work are shown as filled circles while the Cepheid data are from Luck & Lambert (2011). We determine the linear fit, uncertainty, and dispersion about the linear fit to the local and distant open clusters and Cepheids. For the Cepheid data, we superimpose the linear fits to the open cluster data.

kpc). For open clusters with ages ≥ 1.5 Gyr, we find that for all elements except La and Eu, the difference in gradients ([X/H] vs. R_{GC}) between the local and distant samples is significant at the $3\text{-}\sigma$ level or higher. The same result holds when we consider open clusters with ages ≥ 2.5 Gyr. Similarly, we can compare the abundance gradients ([X/H] vs. R_{GC}) for the local and distant Cepheids. In contrast to the open clusters, we find that for all elements, the abundance gradients agree within $1.8\text{-}\sigma$. Furthermore, six of the 12 elements considered show agreement below the $0.9\text{-}\sigma$ level between gradients for the local and distant Cepheids. In summary, the local and distant Cepheids follow the same [X/H] vs. R_{GC} relation. There is, therefore, a fundamental difference in the behavior of radial abundance gradients, [X/H] vs. R_{GC} , between the older open clusters and the Cepheids.

Next, we compare the [X/Fe] radial abundance gradient between the local and distant samples. For the open clusters with ages ≥ 1.5 Gyr, the local and distant samples show the same [X/Fe] vs. R_{GC} gradient with the exceptions of Mn ($2\text{-}\sigma$), La ($3\text{-}\sigma$), and Eu ($3\text{-}\sigma$). When considering the open clusters with ages ≥ 2.5 Gyr, with the exceptions of Mn ($2\text{-}\sigma$) and Eu ($2\text{-}\sigma$), the local and distant samples show the same abundance gradients. A similar comparison for the Cepheids reveals that with the exception of Al ($2\text{-}\sigma$), the local and distant samples show identical abundance gradients for [X/Fe] vs. R_{GC} at the

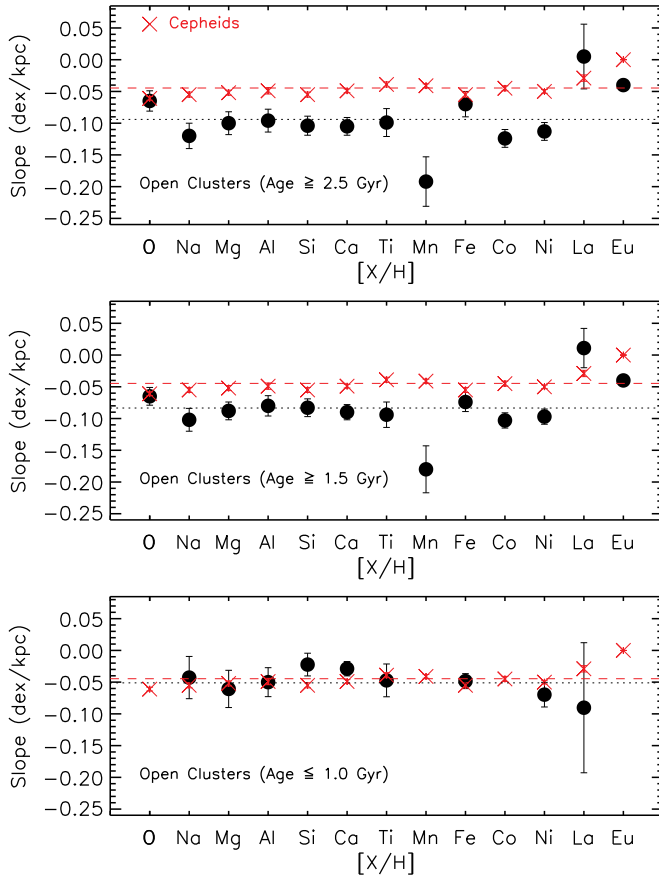


FIG. 32.— Slope of linear fit (dex/kpc) to $[X/H]$ vs. R_{GC} for the open clusters (filled circles) and Cepheids (red crosses) for $R_{GC} < 13$ kpc. The upper, middle, and lower panels show values for open clusters with ages ≥ 2.5 Gyr, ≥ 1.5 Gyr, and ≤ 1.0 Gyr, respectively.

1.8- σ level or lower.

When we consider the trends between $[X/Fe]$ vs. $[Fe/H]$, our qualitative impression is that the local and distant open clusters follow the same relation. Similarly, the local and distant Cepheids appear to follow the same $[X/Fe]$ vs. $[Fe/H]$ relation. Given the moderate ranges in $[Fe/H]$ covered by the distant open cluster and Cepheid samples, these are qualitative rather than quantitative comparisons. For the linear fit to $[X/Fe]$ vs. $[Fe/H]$ across the full data range, we are willing to quantitatively compare the gradients between the open clusters and Cepheids. As before, we assume that the systematic errors in the analysis of a particular type of star will cancel such that we can reliably compare gradients between the two different classes of objects (red giants vs. Cepheids). We find that the open clusters and Cepheids share the same gradients ($< 3\text{-}\sigma$) from the linear fit to $[X/Fe]$ vs. $[Fe/H]$ for all elements except O ($3\text{-}\sigma$), Mn ($4\text{-}\sigma$), and Ni ($3\text{-}\sigma$).

At the risk of over-interpreting these data, the results of this comparison ($[X/Fe]$ vs. $[Fe/H]$) would suggest that the chemical enrichment histories of the older open clusters and Cepheids are surprisingly comparable. This similarity applies to the more metal-rich local samples as well as to the more metal-poor distant samples. Our conclusions would be unchanged had we increased our $[Fe/H]$ ratios by 0.1 dex and decreased our $[X/Fe]$ ratios by 0.1 dex for the open clusters in Paper I and in this study. Similarity in $[X/Fe]$ vs. $[Fe/H]$ relations between local and distant stars that span a large range

in ages cannot be the result of the evolution of a closed system. It remains to be seen how such abundance ratios can be explained within a self-consistent chemical evolution model. One requirement may be the infall of gas onto the outer disk. However, that material must have experienced the same ratio of SNe II to SNe Ia, at a given metallicity, as the gas from which the local disk formed, both at early times (i.e., at the epoch of open cluster formation) and later times when the Cepheids formed.

5. CONCLUSIONS AND FUTURE WORK

Previous papers in this series studied the chemical compositions of open clusters, field stars, and Cepheids in the outer disk. In this paper we present radial velocities and chemical abundances for a new sample of outer disk open clusters. This paper includes the first analysis of the outer disk clusters Be 18 and PWM 4. We compiled a set of chemical abundances for a sample of 49 unique clusters drawn from our studies and from the literature. Using this sample, we studied trends between chemical abundances and distance, age, and metallicity.

We confirm the flattening of the metallicity gradient in the outer disk and that the outer disk open clusters are uniformly metal-poor with super-solar ratios for $[\alpha/Fe]$ and $[Eu/Fe]$. For some elements there are hints that the local ($R_{GC} < 13$ kpc) and distant ($R_{GC} > 13$ kpc) samples may have different radial $[X/Fe]$ abundance gradients.

We confirm that there are no significant trends between metallicity, or abundance ratios $[X/Fe]$, and age (with the likely exception of the s -process elements already noted by D’Orazi et al. 2009 and Maiorca et al. 2011). Compared to a sample of solar neighborhood field giant stars, we find that the open clusters share rather similar trends for $[X/Fe]$ versus $[Fe/H]$ for almost all elements. We quantify the linear trends between $[X/Fe]$ and metallicity and find that the scatter about the mean relation, as low as 0.06 dex for Ni, is comparable to the measurement uncertainties for some elements. For other elements including Co, Zr, Ba, and La, the scatter about the linear trend is significantly higher than the measurement uncertainties which may suggest a real dispersion in abundance ratios. We note that for lines that are strong and/or affected by hyperfine structure (e.g., Ba), the measurement uncertainties may underestimate the true errors. Additionally, some elements including Co and Zr are measured from small numbers of lines such that the measured dispersions are likely larger than the errors from stellar parameter uncertainties alone. Finally, our analysis suggests that this inhomogeneous sample includes ~ 0.1 dex systematic offsets for some elements.

The flattening of the metallicity gradient, differences in metallicity, and the enhancements in $[\alpha/Fe]$ (and perhaps $[Eu/Fe]$) suggest that the outer disk formed from gas with a different star formation history than the solar neighborhood. We reiterate that the individual α elements do not necessarily follow identical patterns. In particular, $[O/Fe]$ and $[Ti/Fe]$ are strongly enhanced in the outer disk relative to the inner disk while $[Mg/Fe]$, $[Si/Fe]$, and $[Ca/Fe]$ show roughly constant ratios as a function of Galactocentric distance. Outer disk field red giant stars, which cover a more limited range in Galactocentric distance, share similar $[X/Fe]$ and $[Fe/H]$ vs. R_{GC} trends as the open clusters at the same range of distances. When compared to Cepheids, the old open clusters (ages ≥ 1.5 Gyr) show steeper $[X/H]$ vs. R_{GC} trends suggesting that the Galactic disk grew via an “inside-out” process. The Cepheids and open clusters share very similar $[X/Fe]$ vs.

[Fe/H] trends. Such similarity between samples of stars with very different ages cannot arise from the chemical evolution of a closed system. Understanding the chemical abundances of old distant open clusters and young distant Cepheids represents a challenge for future chemical evolution models.

Ultimately, a definitive statement about the origin and evolution of the outer disk requires a homogeneous analysis of larger samples of stars in larger numbers of clusters based on high quality spectra. Additional efforts should be undertaken to increase the samples of distant field stars and Cepheids with chemical abundance analyses for a more complete picture of the outer disk. Clearly, the comparison field stars also need to be analyzed on the same system as the open clusters. For example, the work by Przybilla, Nieva, and collaborators (e.g., Przybilla et al. 2008; Nieva & Przybilla 2012) on unevolved early type stars shows that very high precision abundances, 10%, can be obtained for objects spanning a large range in distance. Extremely careful analyses may one day provide similar precision in abundances in open clusters to explore

the origin and evolution of the outer disk.

D.Y. thanks Robert Sharp for assistance with the MPFIT tasks, Sergio Ortolani for providing photometry of PWM 4, Heather Jacobson for sending electronic data, and Giovanni Carraro, Ken Freeman, Brad Gibson, Earl Luck, and Ivan Minchev for helpful discussions. We thank the anonymous referee for thoughtful comments. The authors wish to recognize and acknowledge the very significant cultural role and reverence that the summit of Mauna Kea has always had within the indigenous Hawaiian community. We are most fortunate to have the opportunity to conduct observations from this mountain. We are extremely grateful to the National Science Foundation for their financial support through grants AST 96-19381, AST 99-88156, and AST 03-05431 to the University of North Carolina. DY acknowledges travel support through the Access to Major Research Facilities Program which is supported by the Commonwealth of Australia under the International Science Linkages program. This research has made use of the WEBDA database, operated at the Institute for Astronomy of the University of Vienna.

APPENDIX

A.1 SIGNAL-TO-NOISE CONSIDERATIONS

As noted in Section 4.1, the compilation of open cluster abundances includes data that span a range of S/N (and sample sizes per cluster). We now re-examine whether the trends between [Fe/H] vs. R_{GC} and [X/Fe] vs. R_{GC} change as we make cuts based on S/N.

In Figure 33, we show [Fe/H] vs. R_{GC} again applying a linear fit to the local ($R_{GC} < 13$ kpc) and distant ($R_{GC} > 13$ kpc) samples. In this figure, we show (a) all data, (b) $S/N > 50$, (c) $S/N > 70$, and (d) $S/N > 90$. We find that the slopes and dispersions about the linear fit do not change substantially as we exclude data based on the S/N. One important point we highlight is that for the most stringent cut, $S/N > 90$, there is only one cluster beyond $R_{GC} = 15$ kpc. Panel (d) in this figure underscores the need to re-observe the most distant open clusters at higher S/N ratios in order to obtain more accurate and precise chemical abundance ratios. We also stress the importance of observing multiple stars per cluster, when possible, to increase the statistics and to ensure membership. Indeed, a similar figure could be generated taking into account the S/N, spectral resolution, and number of stars per cluster.

In Figures 34 to 36, we plot [O/Fe], [α /Fe], and [Ni/Fe] vs. R_{GC} . For these representative elements, we again find that the slopes and dispersions about the linear fit to the local and distant samples do not significantly change as we restrict ourselves to only the highest S/N data. Nevertheless, we again argue that accurate and precise chemical abundance measurements are obtained from higher quality spectra and currently, there is a clear need to obtain such data for the most distant open clusters.

A.2 THE TRANSITION FROM INNER TO OUTER DISK

Twarog et al. (1997) were the first to note that the radial abundance distribution, as traced by open clusters, shows a sharp transition near $R_{GC} = 10$ kpc. Numerous studies, including this series of papers, have sought to further understand the transition from the inner to outer disk. The location, and nature, of the transition can potentially provide crucial constraints upon the formation and evolution of the Galactic disk. While most studies have performed quantitative comparisons between the various (chemical) properties of the inner disk and outer disk open clusters, to our knowledge the transition region, or transition radius, is selected in most, if not all, studies through a qualitative visual inspection. In this appendix, we seek to quantify the location of the transition radius between the inner and outer disk.

The data we shall use to quantify the transition radius are [Fe/H] vs. R_{GC} for the complete sample listed in Table 13. We assume that there are two regions, an inner disk and an outer disk. We also assume that each region can be described by a linear relation. Thus, there are five parameters to be determined: (1 and 2) the slope and intercept of the linear fit to the inner disk region, (3 and 4) the slope and intercept of the linear fit to the outer disk region, and (5) the transition radius.

We determine these parameters using the IDL MPFIT routine (Markwardt 2009) which uses the Levenberg-Marquardt technique for least squares minimization. One consideration is that an initial guess for the best parameters is required. On applying the MPFIT routines, this concern appears to be valid. We tested a number of initial guesses for the five parameters. The only parameter that showed a dependence on the initial guess was the transition radius. In the upper panel of Figure 37 we plot the initial guess (which ranges from 9 kpc to 16 kpc in steps of 0.25 kpc) and the optimum value. In this figure, there are two best solutions for the transition radius, 10.4 ± 1.0 kpc and 15.3 ± 1.3 kpc, and the optimum value depends on the choice of initial guess. (The Levenberg-Marquardt technique involves gradient descent. If there is a saddle point, it is therefore not surprising that the final solution depends on our initial guess.) We note that when using either of the two best solutions as the initial guess, their χ^2 values are almost identical, 49.86 (10.4 kpc) and 49.90 (15.3 kpc). In the upper two panels of Figure 38, we overplot the two solutions to our data. The first conclusion we draw from this quantitative analysis is that there does not appear to be a single

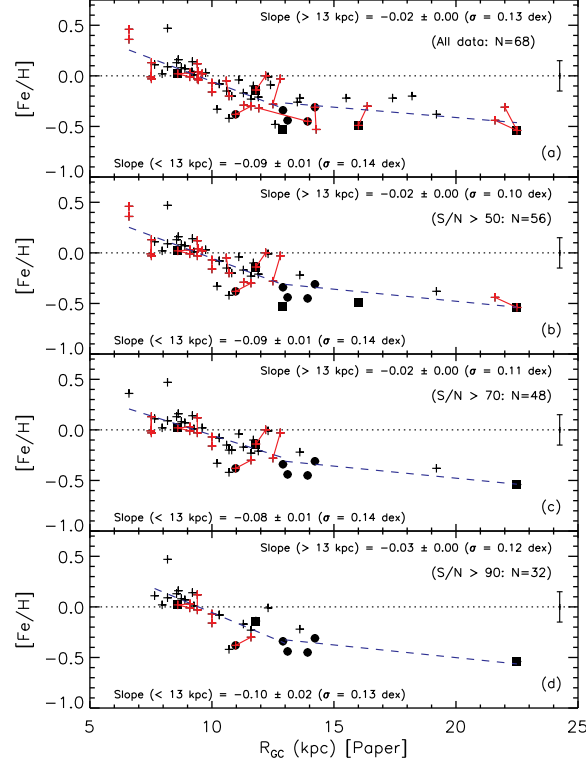


FIG. 33.— $[\text{Fe}/\text{H}]$ vs. R_{GC} for different S/N cuts. From top to bottom, the panels include (a) all clusters, (b) $S/N > 50$, (c) $S/N > 70$, and (d) $S/N > 90$. The symbols are the same as in Figure 19.

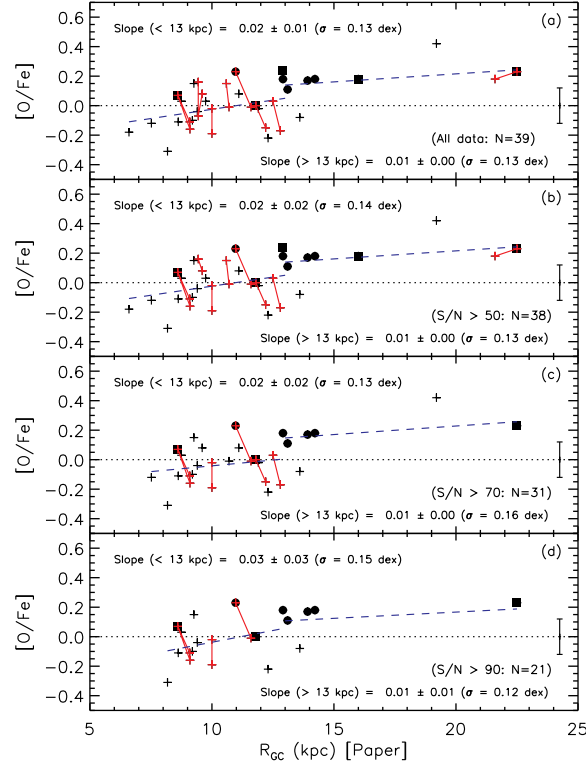
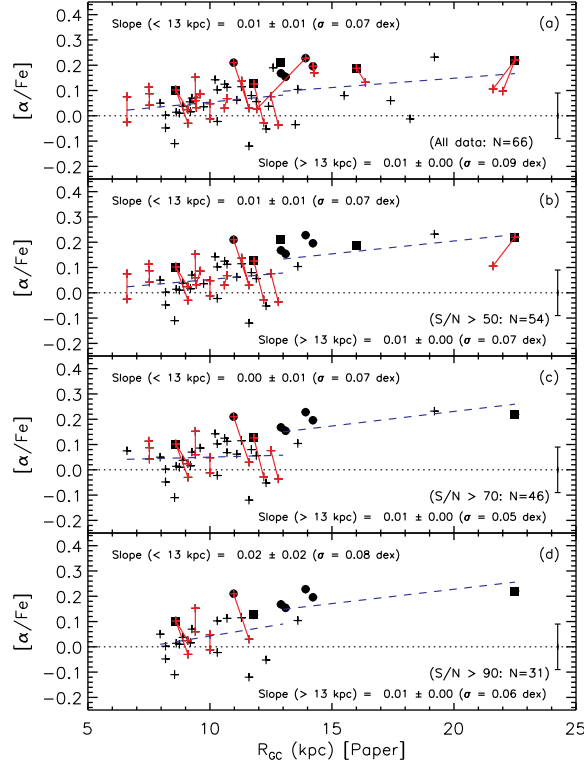
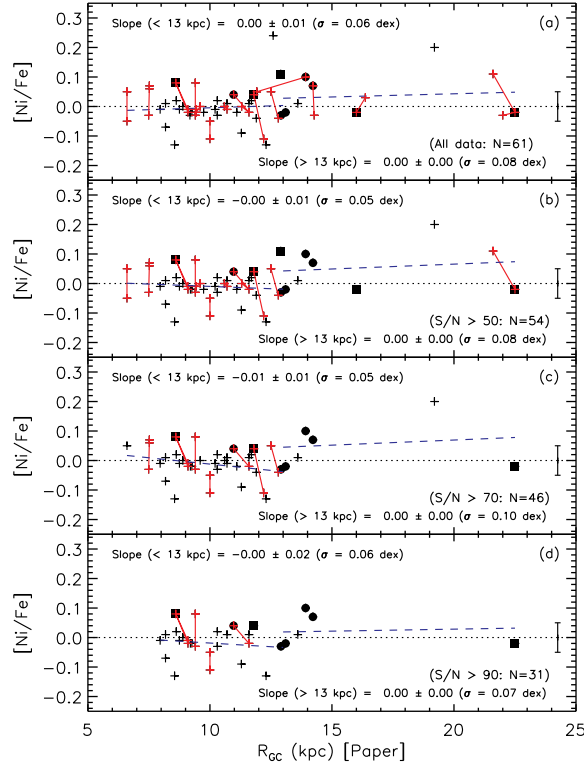


FIG. 34.— Same as Figure 33 but for $[\text{O}/\text{Fe}]$.

value for the optimum transition radius if we do not place any constraints on the linear fits to the inner and outer regions (i.e., Case 1). Rather, there are two equally good solutions for the transition radius at 10.4 ± 1.0 kpc or 15.3 ± 1.3 kpc.

The MPFIT routines include consideration of the errors for the Y axis ($[\text{Fe}/\text{H}]$, for which we adopt a uniform value of 0.15 dex),

FIG. 35.— Same as Figure 33 but for $[\alpha/\text{Fe}]$.FIG. 36.— Same as Figure 33 but for $[\text{Ni}/\text{Fe}]$.

but not for the X axis (R_{GC}). In order to explore the effect of uncertainties in the distances, we adopt a Monte Carlo approach in which we replaced each distance with a random number drawn from a normal distribution of width 0.5 kpc centered at the R_{GC} of the given data point. We repeated this process for each data point in the sample and determined the optimum parameters. We repeated this process for 1,000 new random samples. As above, for each sample we trialed a range of initial guesses for

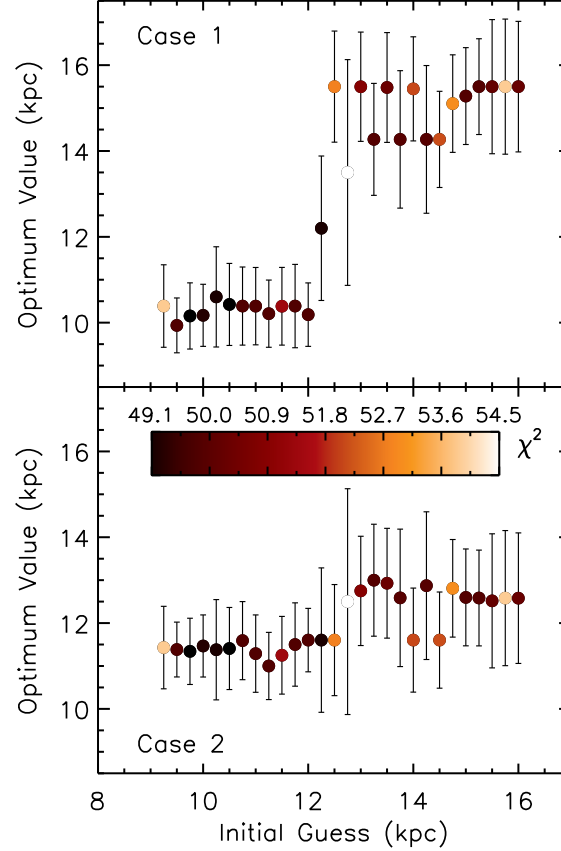


FIG. 37.— Optimum value for the transition radius as a function of the initial guess. Case 1 (upper) is when we do not require the two linear fits to intersect at the transition radius. Case 2 (lower) is when we require the two linear fits to intersect at the transition radius. The colors represent the χ^2 value for each data point.

the transition radius (from 9 kpc to 16 kpc in steps of 0.25 kpc). In the upper panel of Figure 39, we plot the average optimum transition radius as a function of the initial guess. In this figure, the error bars represent the standard deviation of the distribution of 1,000 values. This figure again highlights that there are two preferred values which depend upon the initial guess.

We note that thus far we have not required the two linear fits to intersect at the transition radius. We now consider how the results change if we constrain the two linear functions to intersect at the transition radius (i.e., Case 2), and this may be a more appealing way to describe the behavior of metallicity with Galactocentric distance. In this scenario, there are only four free parameters (the slope and intercept of the fit to the inner region, the transition radius, and the slope of the fit to the outer region). Once again, we test to see whether the optimum value for the transition radius shows a dependence on the initial guess. In the lower panel of Figure 37, there is a suggestion that there are again two solutions which depend on the initial guess, 11.4 ± 0.9 kpc and 12.5 ± 1.1 kpc. In the lower panels of Figure 38, we overplot these two solutions and note again that the χ^2 values (when adopting the optimum values as the initial guesses) for the two solutions are very similar, 50.48 (11.4 kpc) and 51.53 (12.5 kpc).

Finally, we apply the Monte Carlo approach described above to Case 2. In the lower panel of Figure 39 we plot the optimum transition radius as a function of the initial guess where the error bars represent the standard deviation of the distribution of 1,000 values per initial guess and the color-bar represents the average χ^2 . In contrast to Case 1, the Monte Carlo simulations suggest that for Case 2 there is a single best solution for the transition radius of 12.1 ± 0.7 kpc. The second conclusion we draw from this analysis is that if we require the linear fits to the inner and outer regions to intersect at the transition radius, there is a single optimum value for the transition radius of 12.1 ± 0.7 kpc.

Finally, we note that within the uncertainties, the slopes and linear fits we obtain from the MPFIT routines for the inner and outer regions agree with the slopes we measure in the main text based on our qualitatively selected 13 kpc transition radius.

REFERENCES

- Alonso, A., Arribas, S., & Martínez-Roger, C. 1999, *A&AS*, 140, 261
 Alves, D. R. 2000, *ApJ*, 539, 732
 Alves-Brito, A., Meléndez, J., Asplund, M., Ramírez, I., & Yong, D. 2010, *A&A*, 513, A35
 Andrievsky, S. M., Bersier, D., Kovtyukh, V. V., Luck, R. E., Maciel, W. J., Lépine, J. R. D., & Beletsky, Y. V. 2002a, *A&A*, 384, 140
 Andrievsky, S. M., Kovtyukh, V. V., Luck, R. E., Lépine, J. R. D., Bersier, D., Maciel, W. J., Barbuy, B., Klochkova, V. G., Panchuk, V. E., & Karpishev, R. U. 2002b, *A&A*, 381, 32
 Andrievsky, S. M., Kovtyukh, V. V., Luck, R. E., Lépine, J. R. D., Maciel, W. J., & Beletsky, Y. V. 2002c, *A&A*, 392, 491
 Andrievsky, S. M., Luck, R. E., Martin, P., & Lépine, J. R. D. 2004, *A&A*, 413, 159
 Bensby, T., Alves-Brito, A., Oey, M. S., Yong, D., & Meléndez, J. 2010, *A&A*, 516, L13
 —. 2011, *ApJ*, 735, L46
 Bensby, T., Feltzing, S., & Lundström, I. 2004, *A&A*, 421, 969
 Bergemann, M. & Gehren, T. 2008, *A&A*, 492, 823
 Bland-Hawthorn, J., Krumholz, M. R., & Freeman, K. 2010, *ApJ*, 713, 166

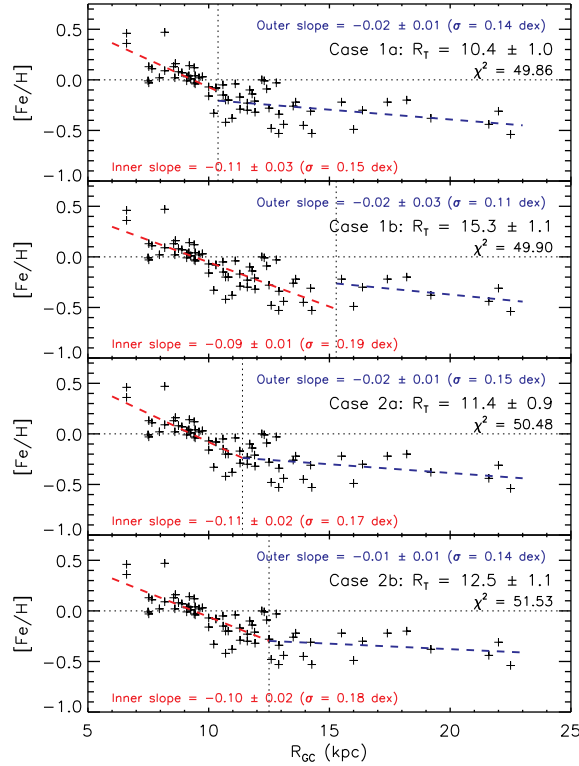


FIG. 38.— $[Fe/H]$ vs. Galactocentric distance for the complete sample. In each panel, we overplot the optimum solution from the MPFIT (Markwardt 2009) routines. Case 1 is when we do not require the linear fits to intersect while Case 2 is when we require the linear fits to intersect. For each case, there are two solutions for the transition radius, depending on the initial guess (see Figure 37). We show the two solutions for each case and note the slope and error, dispersion about the linear fit, the transition radius and error, and χ^2 .

- Bragaglia, A., Carretta, E., Gratton, R. G., Tosi, M., Bonanno, G., Bruno, P., Cali, A., Claudi, R., Cosentino, R., Desidera, S., Farisato, G., Rebescini, M., & Scuderi, S. 2001, *AJ*, 121, 327
- Bragaglia, A., Sestito, P., Villanova, S., Carretta, E., Randich, S., & Tosi, M. 2008, *A&A*, 480, 79
- Bragaglia, A. & Tosi, M. 2006, *AJ*, 131, 1544
- Bresolin, F., Ryan-Weber, E., Kennicutt, R. C., & Goddard, Q. 2009, *ApJ*, 695, 580
- Carney, B. W., Latham, D. W., Stefanik, R. P., & Laird, J. B. 2008, *AJ*, 135, 196
- Carney, B. W., Latham, D. W., Stefanik, R. P., Laird, J. B., & Morse, J. A. 2003, *AJ*, 125, 293
- Carney, B. W., Lee, J.-W., & Dodson, B. 2005a, *AJ*, 129, 656
- Carney, B. W., Yong, D., Teixeira de Almeida, M. L., & Seitzer, P. 2005b, *AJ*, 130, 1111
- Carraro, G., Bresolin, F., Villanova, S., Matteucci, F., Patat, F., & Romaniello, M. 2004, *AJ*, 128, 1676
- Carrera, R. & Pancino, E. 2011, *A&A*, 535, A30
- Carretta, E., Bragaglia, A., & Gratton, R. G. 2007, *A&A*, 473, 129
- Carretta, E., Bragaglia, A., Gratton, R. G., & Tosi, M. 2004, *A&A*, 422, 951
- , 2005, *A&A*, 441, 131
- Cescutti, G., Matteucci, F., François, P., & Chiappini, C. 2007, *A&A*, 462, 943
- Chen, L., Hou, J. L., & Wang, J. J. 2003, *AJ*, 125, 1397
- Chiappini, C., Matteucci, F., & Romano, D. 2001, *ApJ*, 554, 1044
- Costa, R. D. D., Uchida, M. M. M., & Maciel, W. J. 2004, *A&A*, 423, 199
- Daflon, S. & Cunha, K. 2004, *ApJ*, 617, 1115
- De Silva, G. M., Freeman, K. C., Asplund, M., Bland-Hawthorn, J., Bessell, M. S., & Collet, R. 2007, *AJ*, 133, 1161
- de Silva, G. M., Gibson, B. K., Lattanzio, J., & Asplund, M. 2009, *A&A*, 500, L25
- De Silva, G. M., Snenen, C., Paulson, D. B., Asplund, M., Bland-Hawthorn, J., Bessell, M. S., & Freeman, K. C. 2006, *AJ*, 131, 455
- D'Orazi, V., Bragaglia, A., Tosi, M., Di Fabrizio, L., & Held, E. V. 2006, *MNRAS*, 368, 471
- D'Orazi, V., Magrini, L., Randich, S., Galli, D., Busso, M., & Sestito, P. 2009, *ApJ*, 693, L31
- Freeman, K. & Bland-Hawthorn, J. 2002, *ARA&A*, 40, 487
- Friel, E. D. 1995, *ARA&A*, 33, 381
- Friel, E. D., Jacobson, H. R., & Pilachowski, C. A. 2005, *AJ*, 129, 2725
- , 2010, *AJ*, 139, 1942
- Friel, E. D., Janes, K. A., Tavaréz, M., Scott, J., Katsanis, R., Lotz, J., Hong, L., & Miller, N. 2002, *AJ*, 124, 2693
- Fu, J., Hou, J. L., Yin, J., & Chang, R. X. 2009, *ApJ*, 696, 668
- Fulbright, J. P., McWilliam, A., & Rich, R. M. 2007, *ApJ*, 661, 1152
- Gratton, R., Snenen, C., & Carretta, E. 2004, *ARA&A*, 42, 385
- Haywood, M. 2008, *MNRAS*, 388, 1175
- Hill, V. & Pasquini, L. 1999, *A&A*, 348, L21
- Hou, J. L., Prantzos, N., & Boissier, S. 2000, *A&A*, 362, 921
- Jacobson, H. R. 2009, PhD thesis, Indiana University
- Jacobson, H. R., Friel, E. D., & Pilachowski, C. A. 2008, *AJ*, 135, 2341
- , 2009, *AJ*, 137, 4753
- , 2011a, *AJ*, 141, 58
- Jacobson, H. R., Pilachowski, C. A., & Friel, E. D. 2011b, *AJ*, 142, 59
- Janes, K. A. 1979, *ApJS*, 39, 135
- Jilková, L., Carraro, G., Jungwiert, B., & Minchev, I. 2012, *A&A*, 541, A64
- Kaluzny, J. 1994, *A&AS*, 108, 151
- , 1997, *A&AS*, 121, 455
- Kaluzny, J. & Mazur, B. 1991, *Acta Astronomica*, 41, 167
- Kobayashi, C. & Nakasato, N. 2011, *ApJ*, 729, 16
- Kurucz, R. 1993, *ATLAS9 Stellar Atmosphere Programs and 2 km/s grid*. Kurucz CD-ROM No. 13. Cambridge, Mass.: Smithsonian Astrophysical Observatory, 1993., 13
- Lemasle, B., François, P., Piersimoni, A., Pedicelli, S., Bono, G., Laney, C. D., Primas, F., & Romaniello, M. 2008, *A&A*, 490, 613
- Lind, K., Asplund, M., & Barklem, P. S. 2009, *A&A*, 503, 541
- Lind, K., Asplund, M., Barklem, P. S., & Belyaev, A. K. 2011, *A&A*, 528, A103
- Luck, R. E., Andrievsky, S. M., Kovtyukh, V. V., Gieren, W., & Graczyk, D. 2011, *AJ*, 142, 51
- Luck, R. E., Gieren, W. P., Andrievsky, S. M., Kovtyukh, V. V., Fouqué, P., Pont, F., & Kienle, F. 2003, *A&A*, 401, 939
- Luck, R. E. & Heiter, U. 2007, *AJ*, 133, 2464
- Luck, R. E. & Lambert, D. L. 2011, *AJ*, 142, 136
- Maciel, W. J. & Costa, R. D. D. 2009, in *IAU Symposium*, Vol. 254, IAU Symposium, ed. J. Andersen, J. Bland-Hawthorn, & B. Nordström, 38P
- Maciel, W. J., Costa, R. D. D., & Uchida, M. M. M. 2003, *A&A*, 397, 667
- Magrini, L., Sestito, P., Randich, S., & Galli, D. 2009, *A&A*, 494, 95
- Maiorca, E., Magrini, L., Busso, M., Randich, S., Palmerini, S., & Trippella, O. 2012, *ApJ*, 747, 53
- Maiorca, E., Randich, S., Busso, M., Magrini, L., & Palmerini, S. 2011, *ApJ*, 736, 120
- Markwardt, C. B. 2009, in *Astronomical Society of the Pacific Conference Series*, Vol. 411, *Astronomical Data Analysis Software and Systems XVIII*, ed. D. A. Bohlender, D. Durand, & P. Dowler, 251

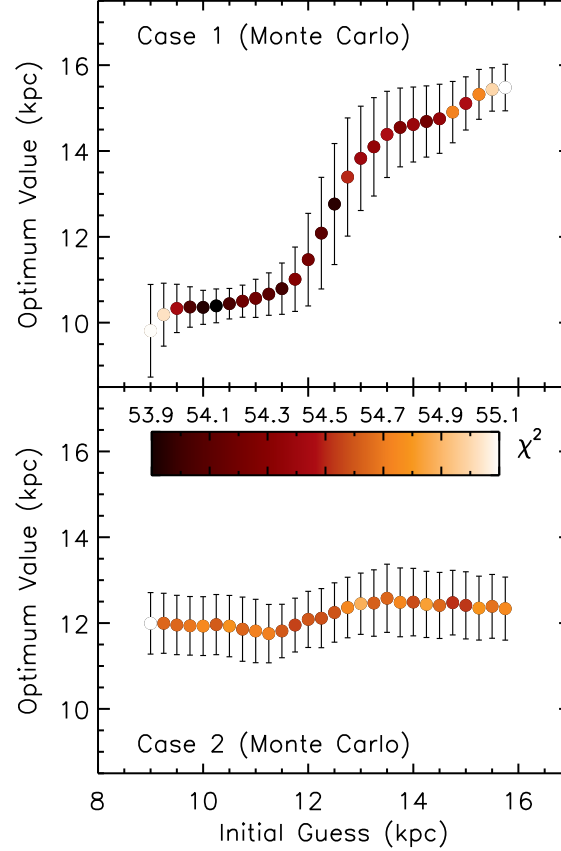


FIG. 39.— Same as Figure 37 but based on a Monte Carlo simulation for $N = 1,000$ realizations. In each realization, the R_{GC} for a given data point was replaced by a random number drawn from a normal distribution of width 0.5 kpc centered at the original value. The data and error bars represent the average value and dispersion from the 1,000 realizations respectively. The colors represent the average χ^2 at each data point.

- Minchev, I., Famaey, B., Combes, F., Di Matteo, P., Mouhcine, M., & Wozniak, H. 2011, *A&A*, 527, A147
- Minchev, I., Famaey, B., Quillen, A. C., Di Matteo, P., Combes, F., Vlahic, M., Erwin, P., & Bland-Hawthorn, J. 2012, *arXiv* 1203.2621
- Nieva, M.-F. & Przybilla, N. 2012, *A&A*, 539, A143
- Önehag, A., Korn, A., Gustafsson, B., Stempels, E., & Vandenberg, D. A. 2011, *A&A*, 528, A85
- Ortolani, S., Bica, E., & Barbuy, B. 2005, *A&A*, 437, 531
- Pancino, E., Carrera, R., Rossetti, E., & Gallart, C. 2010, *A&A*, 511, A56
- Paulson, D. B., Sneden, C., & Cochran, W. D. 2003, *AJ*, 125, 3185
- Pedicelli, S., Bono, G., Lemasle, B., François, P., Groenewegen, M., Lub, J., Pel, J. W., Laney, D., Piersimoni, A., Romaniello, M., Buonanno, R., Caputo, F., Cassisi, S., Castelli, F., Leurini, S., Pietrinferni, A., Primas, F., & Pritchard, J. 2009, *A&A*, 504, 81
- Pilkington, K., Few, C. G., Gibson, B. K., Calura, F., Michel-Dansac, L., Thacker, R. J., Mollá, M., Matteucci, F., Rahimi, A., Kawata, D., Kobayashi, C., Brook, C. B., Stinson, G. S., Couchman, H. M. P., Bailin, J., & Wadsley, J. 2012, *A&A*, 540, A56
- Przybilla, N., Nieva, M., & Butler, K. 2008, *ApJ*, 688, L103
- Ramírez, I. & Meléndez, J. 2005, *ApJ*, 626, 465
- Rieke, G. H. & Lebofsky, M. J. 1985, *ApJ*, 288, 618
- Roškar, R., Debattista, V. P., Stinson, G. S., Quinn, T. R., Kaufmann, T., & Wadsley, J. 2008, *ApJ*, 675, L65
- Salaris, M., Weiss, A., & Percival, S. M. 2004, *A&A*, 414, 163
- Sánchez-Blázquez, P., Courty, S., Gibson, B. K., & Brook, C. B. 2009, *MNRAS*, 398, 591
- Schönrich, R. & Binney, J. 2009, *MNRAS*, 396, 203
- Scott, J. E., Friel, E. D., & Janes, K. A. 1995, *AJ*, 109, 1706
- Sellwood, J. A. & Binney, J. J. 2002, *MNRAS*, 336, 785
- Sestito, P., Bragaglia, A., Randich, S., Carretta, E., Prisinzano, L., & Tosi, M. 2006, *A&A*, 458, 121
- Sestito, P., Bragaglia, A., Randich, S., Pallavicini, R., Andrievsky, S. M., & Korotin, S. A. 2008, *A&A*, 488, 943
- Sestito, P., Randich, S., & Bragaglia, A. 2007, *A&A*, 465, 185
- Simmerer, J., Sneden, C., Cowan, J. J., Collier, J., Woolf, V. M., & Lawler, J. E. 2004, *ApJ*, 617, 1091
- Skrutskie, M. F., Cutri, R. M., Stiening, R., Weinberg, M. D., Schneider, S., Carpenter, J. M., Beichman, C., Capps, R., Chester, T., Elias, J., Huchra, J., Liebert, J., Lonsdale, C., Monet, D. G., Price, S., Seitzer, P., Jarrett, T., Kirkpatrick, J. D., Gizis, J. E., Howard, E., Evans, T., Fowler, J., Fullmer, L., Hurt, R., Light, R., Kopan, E. L., Marsh, K. A., McCallon, H. L., Tam, R., Van Dyk, S., & Wheelock, S. 2006, *AJ*, 131, 1163
- Sneden, C. 1973, *ApJ*, 184, 839
- Tolstoy, E., Hill, V., & Tosi, M. 2009, *ARA&A*, 47, 371
- Tosi, M., Pulone, L., Marconi, G., & Bragaglia, A. 1998, *MNRAS*, 299, 834
- Twarog, B. A., Ashman, K. M., & Anthony-Twarog, B. J. 1997, *AJ*, 114, 2556
- Villanova, S., Carraro, G., Bresolin, F., & Patat, F. 2005, *AJ*, 130, 652
- Vlahić, M., Bland-Hawthorn, J., & Freeman, K. C. 2009, *ApJ*, 697, 361
- . 2011, *ApJ*, 732, 7
- Vogt, S. S., Allen, S. L., Bigelow, B. C., Bresee, L., Brown, B., Cantrall, T., Conrad, A., Couture, M., Delaney, C., Epps, H. W., Hilyard, D., Hilyard, D. F., Horn, E., Jern, N., Kanto, D., Keane, M. J., Kibrick, R. I., Lewis, J. W., Osborne, J., Pardeilhan, G. H., Pfister, T., Ricketts, T., Robinson, L. B., Stover, R. J., Tucker, D., Ward, J., & Wei, M. Z. 1994, in *Society of Photo-Optical Instrumentation Engineers (SPIE) Conference Series*, Vol. 2198, Society of Photo-Optical Instrumentation Engineers (SPIE) Conference Series, ed. D. L. Crawford & E. R. Craine, 362
- Worthey, G., España, A., MacArthur, L. A., & Courteau, S. 2005, *ApJ*, 631, 820
- Yong, D., Carney, B. W., & Teixeira de Almeida, M. L. 2005, *AJ*, 130, 597
- Yong, D., Carney, B. W., Teixeira de Almeida, M. L., & Pohl, B. L. 2006, *AJ*, 131, 2256